Petrogenesis of Pseudocarbonatites in the Bancroft Region, Southwestern Grenville Province

by

Alisia Tien Mar

A thesis
presented to the University of Waterloo
in fulfillment of the
thesis requirements for the degree of
Master of Science
in
Earth Sciences

Waterloo, Ontario, Canada, 2022

Author's Declaration

This thesis consists of material all of which I authored or co-authored: see Statement of Contributions included in the thesis. This is a true copy of the thesis, including any required final revisions, as accepted by my examiners.

I understand that my thesis may be made electronically available to the public.

Statement of Contributions

All field and petrographic observations are my own. Carson Kinney and Jillian Kendrick assisted in sample collection. Thick sections were prepared by me, and Nina Hening (Department of Chemistry, University of Waterloo) assisted with the SEM-EDX analyses. I prepared calcite samples for isotope analysis. Carbon, oxygen, and strontium isotopes of calcite samples were measured by staff at the EIL laboratory (University of Waterloo). I did the wet chemistry to prepare the samples for trace element analysis. Sarah McCaugherty (Department of Earth and Environmental Sciences, University of Waterloo) assisted with the ICP-MS analyses. I wrote this thesis with comments and edits from my supervisor, Chris Yakymchuk (Department of Earth and Environmental Science, University of Waterloo).

Abstract

Carbonatites are rare igneous rocks that form from fractionation of carbonate-rich, silica undersaturated magma. The petrogenesis of pseudocarbonatites (rocks that are similar to carbonatites, but without a clear mantle link) is less clear. Pseudocarbonatites may be derived from fractionation of mantle-derived magmas (like carbonatites) or generated from partial melting of carbonate rocks of a sedimentary origin (e.g., limestone). This thesis investigates a suite of Proterozoic pseudocarbonatites from Bancroft (Ontario) in the southwestern Grenville Province. I test the hypothesis that pseudocarbonatites were derived from partial melting of metasedimentary rocks in the region using petrology, whole-rock trace element geochemistry, and stable isotope analysis. Concentrations of Rare Earth Elements and other trace elements in the pseudocarbonatites are inconsistent with values from carbonatites or nearby nepheline syenites, but closely resemble those of marbles in the region. Carbon and oxygen isotope ratios of pseudocarbonatites are also inconsistent with North American carbonatites or a mantle origin and strontium isotope ratios are higher than average Ontario carbonatites. However, strontium isotopic ratios are broadly compatible with the values of marbles in the region. Therefore, the pseudocarbonatites were most likely generated during partial melting of marbles during fluid-influx associated with Grenville orogenesis. This suggests that carbon can be remobilized as carbonate melt during high-temperature metamorphism, which has implications for understanding the movement of carbon through the Earth's crust and the carbon cycle of the geosphere.

Acknowledgements

I would like to thank my supervisor, Chris Yakymchuk, for providing me with positive feedback and always supporting not only my work but also my mental health. I could not have been successful with this thesis without him. Thank you to the Yakymchuk research group, the "Yak Pak", for all their welcoming kindness and their readiness to lend a hand. I would also like to thank my family and friends for their continued encouragement and a special thank you to my boyfriend Wesley who always believes in me even when I do not believe in myself.

Dedication

I dedicate this thesis to Emily Damianoff, a friend who always provides support and understanding. Thank you for being one of my first “geology friends” and for spending long days in the field staring at outcrops with me.

Table of Contents

List of Figures

List of Tables

List of Abbreviations

The mineral abbreviations used in this thesis are from (Whitney and Evans, 2010) and are summarized below:

Amp.....amphibole

Bt.....biotite

Cal.....calcite

Cpx.....clinopyroxene

Dol .....dolomite

Fsp .....feldspar

Ms .....muscovite

Nph.....nepheline

Qz.....quartz

Ttn.....titanite

Wo.....wollastonite

1.0 Introduction

1.1 Carbon mobility in the lithosphere

With the growing concerns of the attribution of atmospheric carbon dioxide (CO_2) to global climate change (Brovkin et al., 2004; Eamus and Jarvis, 1989; Manabe and Stouffer, 1980), there is a strong incentive to better understand all aspects of carbon cycling on Earth. The global carbon cycle focuses primarily on the interaction of carbon in the atmosphere, oceans, and shallow crustal environments, but relatively little is known about the deep carbon cycle and carbon movement generated by the metamorphic carbon cycle (Hazen and Schiffries, 2013) (Figure 1.1). The annual metamorphic carbon cycle is generally considered to be at steady-state with a carbon flux of ~0.01% of the atmospheric carbon reservoir (Gaillardet and Galy, 2008). However, there is evidence that this only holds true for the longest time scales (Evans, 2011). For example, at short timescales the Himalayan orogenic records metamorphic processes that are not in equilibrium with the rest of the carbon cycle and can cause an imbalance in the output/input of carbon in the atmosphere (Evans, 2011). The movement of carbon through Earth's lithosphere is poorly understood (Hazen and Schiffries, 2013), but is a critical facet in understanding how carbon is cycled on Earth.

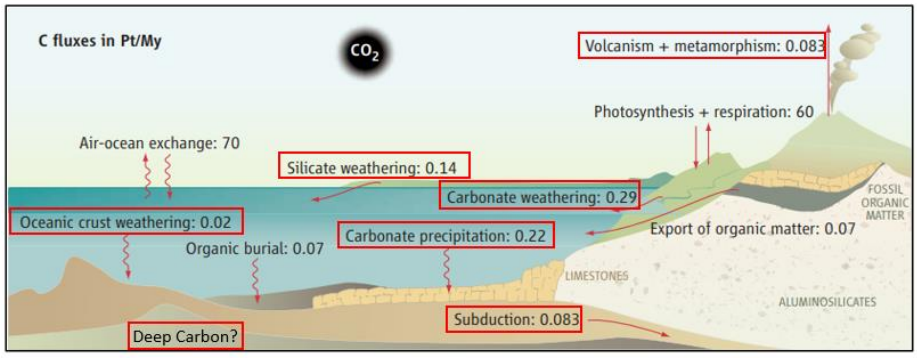

Figure 1.1. Carbon cycle modified from Gillardet and Galy (2008). Red boxes outline parts of the rock cycle.

Movement of carbon in Earth's lithosphere can be broken down into three processes: metamorphic decarbonation reactions (e.g., Stewart et al., 2019), the generation of carbon-rich igneous rocks through magmatic fractionation (e.g., Bailey, 1974; Li et al., 2018), and the partial melting of calcareous rocks (e.g., Chiarenzelli et al., 2019). Each of these can require different pressure-temperature conditions and therefore can affect different regions of Earth's crust undergoing various tectonic processes. Some of these processes require the presence of specific metamorphic protoliths (e.g., chemical sedimentary carbonates) whereas others are igneous and require rare thermochemical conditions to form, such as *natrocarbonatites* in Oldoninyo Lengai in the Tanzanian rift valley (Keller and Kraft, 1990).

Decarbonation reactions occur when the combination of carbonate minerals and silicate minerals form new carbonate minerals and generate CO_2 as a product (Figure 1.2) (Stewart et al., 2019). An example of a decarbonation reaction is shown in reaction (1). Increasing temperatures drive decarbonation reactions because carbonate-silicate mineral assemblages (such as calcite ($CaCO_3$) and quartz (SiO_2)) are only stable together at lower temperatures at a given pressure and fluid composition (Figure 1.2) (Stewart et al., 2019). Rarely, these reactions can occur in the absence of silicate minerals when a carbonate mineral breaks down into a mineral oxide and CO_2 (Stewart et al., 2019). These reactions generally occur when rocks with carbonate and silicate minerals undergo a significant increase in temperature and pressure (Bowen, 1940; Goldschmidt, 1912; Harker and Tuttle, 1956; Stewart et al., 2019).

$$CaCO_{3\ (calcite)} + SiO_{2\ (quartz)} \rightarrow CaSiO_{3\ (wollastonite)} + CO_{2\ (fluid)} \quad (1)$$

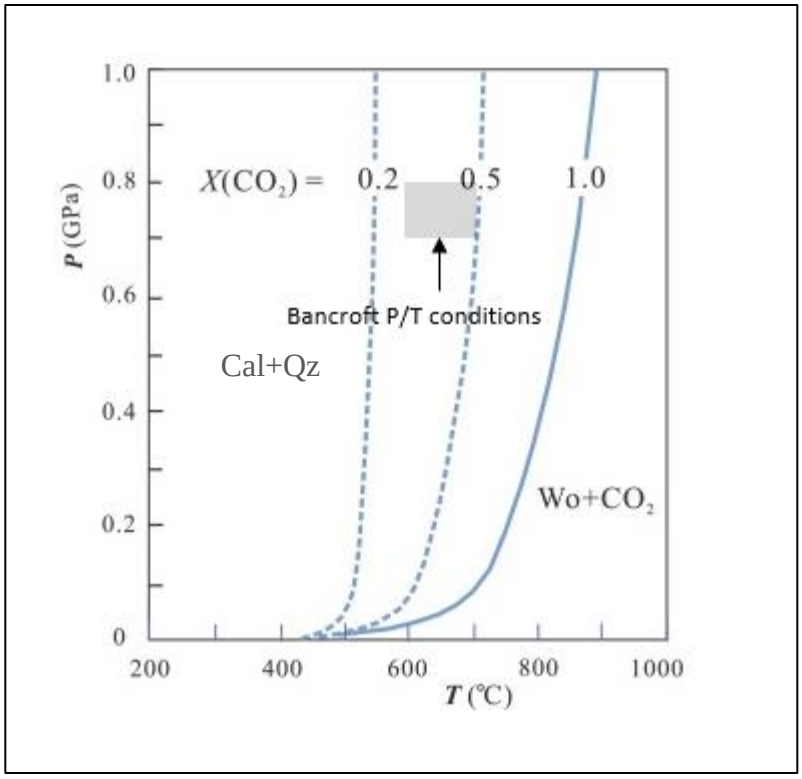

Figure 1.2. P/T diagram of the common quartz-calcite decarbonation reaction modified from Bucher and Grapes (2011). Metamorphic CO_2 can be generated over a wide array of pressures and temperatures depending on the composition of the fluid. $X(CO_2)$ is the molar proportion of CO_2 in the fluid ($X(CO_2)$ = molar (CO_2 + H_2O)). Bancroft P/T conditions are from Streepey et al. (1997).

Another mechanism that mobilizes carbon in the lithosphere is the generation of carbonate-rich igneous rocks from the mantle. Igneous rocks are mainly composed of silicate-minerals, but carbonate-rich igneous rocks exist as carbonatites (Mitchell, 2005). Carbonatites (*sensu stricto*) are defined as igneous rocks that contain >50% primary (magmatic) carbonate minerals (Le Maitre et al., 2005). Generally, carbonatitic magma is generated in extensional tectonic environments due to the partial melting of metasomatized mantle (Bailey, 1974; Li et al., 2018). In rare cases, carbonatite volcanism occurs producing *natrocarbonatites* (Keller and Kraft, 1990). The only known modern carbonatite volcanic systems are formed in Lengai, Tanzania from a sodium carbonate magma (Keller and Kraft, 1990).

Partial melting of calcareous rocks is the least understood component of carbon movement in the lithosphere but may be more common in the crust than previously thought (Ferrero et al., 2016). High temperature metamorphism or interaction with hydrothermal fluids can partially melt calcareous rocks and mobilize the carbon within them (e.g., Floess et al., 2015; Liu et al., 2006). For example, in the northern Baikal region of Russia, mafic magma was contaminated by the partial melting of dolomitic xenoliths, from the rapid heating of the xenoliths, producing a calcite-rich melt (Wenzel et al., 2001). In New-Carlisle, Quebec, partial melting occurred at the intrusive contact between large mafic dykes and clastic sediments generating carbonate melts as superheated fluids infiltrated the sediments from the mafic dykes (Jutras et al., 2006). Partial melting of calcareous rocks can result in the formation of *pseudocarbonatites*, which are mineralogically and texturally similar to carbonatites (*sensu stricto*) (Mitchell, 2005). The main difference between pseudocarbonatites and carbonatites is how they are formed; pseudocarbonatites form through partial melting (anatexis) of carbonate rocks during high-temperature metamorphism and carbonatites from crystallization of mantle-derived carbonatitic magma (Mitchell, 2005). Partial melting of carbonates is expected to occur during high-temperature metamorphism in the deep crust (Floess et al., 2015). Although exposures of the deep crust are rare, they are out best analogue for understanding the processes that can mobilize carbon in the deep portions of the Earth's continents.

1.2 Carbonatites and pseudocarbonatites

Carbonatites are igneous rocks composed of more than 50 modal % primary (magmatic) carbonate and containing less than 20 weight % SiO_2 (Le Maitre et al., 2005). This definition does not consider the petrogenesis of carbonatites and instead groups them entirely based on modal mineralogy (Mitchell, 2005). Carbonatites form at mantle depths or through extreme differentiation of mantle-related silicic magmas at crustal levels (Mitchell, 2005). Each magma type and their associated carbonatite form at different depths by different degrees of partial melting and have differentiating geochemical characteristics (Stewart et al., 2019).

Carbonatites are enriched in Large Ion Lithophile Elements (LILE) like Ba, Th, and Sr and light rare earth elements (LREE) and contain lower amounts of Cs, Rb, K, and heavy rare earth elements (HREE) (Nelson et al., 1988). Carbonatites have mineral assemblages that are mainly carbonate minerals (calcite, ankerite, and dolomite), with minor amounts of clinopyroxene, Na-Ca rich amphibole (richterite), biotite, apatite, and magnetite (Mitchell, 2005). They are relatively rare although more examples continue to be found around the world (e.g., Woolley and Kjarsgaard, 2008).

A sub-group of carbonatites that are not formed by differentiation of mantle-derived magmas but are formed at crustal depths are called a *pseudocarbonatites* (Mitchell, 2005). The mineral assemblages and microstructures of igneous carbonatites and pseudocarbonatites can be very similar and therefore they can be difficult to distinguish from one another in the field. Their main differences come from their petrogenesis.

The genetic model for carbonatites is that they form from a carbonatitic magma produced from very low degrees of partial melting in the mantle that was metasomatized in the mantle wedge above a subduction zone (Li et al., 2018) (Figure 1.3). Current hypotheses for the magma

generation include residual melt from fractionated carbonated nephelinte or melilitite, immiscible melt fractions of CO_2 saturated silicate melts, and primary mantle melts generated through partial melting of CO_2 bearing peridotite (Jones et al., 2013). The genetic model for pseudocarbonatites is that they are produced from partial melting of carbonate rocks in the crust (Mitchell, 2005). This is not always feasible in the crust because calcite has a high melting point (>1300^{o}C), however partial melting of carbonate rocks is possible at much lower temperatures that are found at middle to deep crustal conditions when H_2O-rich fluids can be present (Durand et al., 2015).

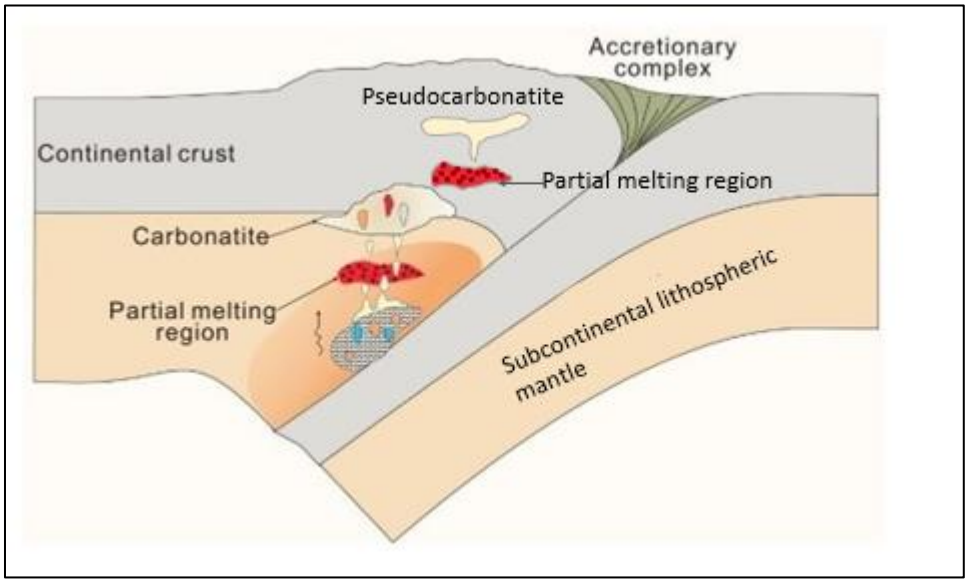

Figure 1.3. Genetic model of carbonatites formation in the sub-continental lithospheric mantle wedge above a subduction zone. Modified from Li et al. (2018). Pseudocarbonatites can form in the deep continental crust.

1.3 Origin of calcite-rich rocks in the Bancroft Region

This thesis investigates the origin of rocks with similar mineralogy to carbonatites and pseudocarbonatites found in the Bancroft domain in southeastern Ontario. These rocks have unknown petrogenetic histories. To avoid the genetic connotations of the terms *carbonatite* and *pseudocarbonatite*, the descriptive (i.e. non-genetic) term "calcite-rich rocks" will be used for these rocks for the remainder of this thesis. The goal of this thesis is to determine the petrogenesis of these rocks to discern if they are carbonatites or pseudocarbonatites.

Calcite-rich rocks in the Bancroft area are similar to rocks from neighbouring regions in the Grenville Province and the Adirondacks. Calcite-rich rocks from Bancroft were first classified as pegmatitic vein dikes by Ellsworth (1932). Hypotheses for the calcite-rich rocks in the Grenville Province include crystallization from a depleted mantle source (Moecher et al., 1997), solid-state ductile flow of remobilized marbles (Moyd, 1990), and anatexis (partial melting) of metasedimentary rocks (Chiarenzelli et al., 2019).

A depleted mantle origin of calcite-rich lithologies in the Central Metasedimentary Belt boundary zone (CMBbz) in the Grenville Province in Ontario was proposed by Moecher et al. (1997). These observations are based on Nd isotopic compositions consistent with a depleted mantle source and petrologic and geochemical characteristics that are similar to carbonatites (Moecher et al., 1997).

Remobilized marbles were proposed by Moyd (1990) to explain rocks with calc-silicate minerals in Bancroft, Ontario. Metamorphosed marbles can exhibit ductile flow (solid state) though different lithologies and emplace into fractures as calcite-rich rocks (Moyd, 1990). Given the low strength of marble compared to most other rock types (e.g., De Bresser et al., 2002), high temperature metamorphism could lead to ductile marble migration and interaction with rocks

during movement which would allow the marble to acquire varying mineral assemblages before final emplacement.

Another hypothesis for the petrogenesis of calcite-rich rocks is the partial melting of metasedimentary bedrock during widespread (i.e., non-local) anatexis driven by the influx of fluids and volatiles during rapid uplift and exhumation (Chiarenzelli et al., 2019). This is indicated by $\delta^{18}O$ and $\delta^{13}C$ values that range from typical mantle-derived carbonatites to those of sedimentary carbonate rocks and marbles.

The rock types of interest for this thesis are metasedimentary rocks (marbles) and calcite-rich rocks (of unknown petrogenesis) around the town of Bancroft, Ontario. This thesis will test the hypothesis that the calcite-rich rocks were derived from partial melting (anatexis) of carbon-rich metasedimentary rocks (e.g., marbles and/or calc-silicate rocks) and are therefore pseudocarbonatites (cf. Mitchell, 2005). The hypothesis is tested by combining fieldwork, microscopy, isotope analysis, and rare earth element and trace element geochemistry. This will provide new insights into: (1) the origin of calcite-rich rocks in the Bancroft region, (2) partial melting of metasedimetary rocks during regional metamorphism associated with the Proterozoic Grenville orogen, and (3) addressing if similar reactions could be occurring in analogous modern orogenic systems, such as in the modern Himalaya-Tibet system.

1.4 Outline of thesis

This thesis is divided into seven additional sections. Section 2.0 outlines the specific research objectives of this thesis. Section 3.0 reviews the geological setting of the Bancroft Region and section 4.0 presents the analytical methods. Section 5.0 reports the results of field and petrographic observations as well as geochemical and isotopic data of samples. Section 6.0 discusses the origin and petrogenesis of calcite-rich rocks in the Bancroft region and explores the consequences for carbon mobility in the crust. Section 7.0 summarized the conclusions of this thesis and section 8.0 provides suggested avenues for future research.

2.0 Research Objectives

The purpose of this study is to determine the petrogenesis of calcite-rich rocks found in the Bancroft area of the southwestern Grenville Province and test the hypothesis that they were derived from partial melting of Grenville carbonate-rich metasedimentary rocks. This hypothesis will be tested by examining field relationships, observing microscopic relationships through optical microscopy, and obtaining geochemical data that includes O, C, and Sr isotope analysis as well as concentrations of rare earth elements and other trace elements.

3.0 Geological Setting

3.1 Grenville orogen and Grenville Province

The Grenville orogeny was a Himalayan scale orogenic event that occurred during the formation of the supercontinent Rodinia when the continents Laurentia and Amazonia collided at 1090–980 Ma (Rivers et al., 2012). The Grenville Orogen extends from Canada through the United States and into Mexico (Hoffman, 1988, 1989) (Figure 3.1). Grenvillian-aged rocks have also been recognized in the Caledonian orogen of Northern Ireland and Scotland, and in the Syeconorwegian Province in Norway (Davidson et al., 1998). There is evidence that the Grenville Orogen continues from Central America to Antarctica (Karlstrom et al., 1999) and from India to Australia with Grenville-aged high-temperature metamorphic rocks found throughout the South American Andes (e.g., Yakymchuk et al., 2019).

The Grenville Orogen is divided into four domains; the southern extent in Texas and Mexico, the basement of the Appalachians found mostly in Newfoundland, the Adirondacks on the New York, USA-Canada border, and the Grenville Province of Ontario, Quebec, and the northern USA. The Grenville Province is the longest continuous segment of a late Mesoproterozoic belt that is found globally (Tollo et al., 2004). It is composed of high-grade metamorphic gneiss complexes with evidence of ductile deformation and partial melting and contains the largest known anorthositic intrusions in the world (Ashwal and Wooden, 1983). The Grenville Province is the most studied locality of the entire Grenville Orogen and is best exposed in eastern Canada and the northern USA (Figure 3.1). This region is an ideal study area because there is no regional metamorphic overprinting since the dominant orogenic event in the late Mesoproterozoic. It is also one of the best exposed areas in the world for investigating high-temperature metamorphism and

melting of carbonate rocks because of the scarcity of metamorphosed Proterozoic carbonate rocks in deep crustal settings.

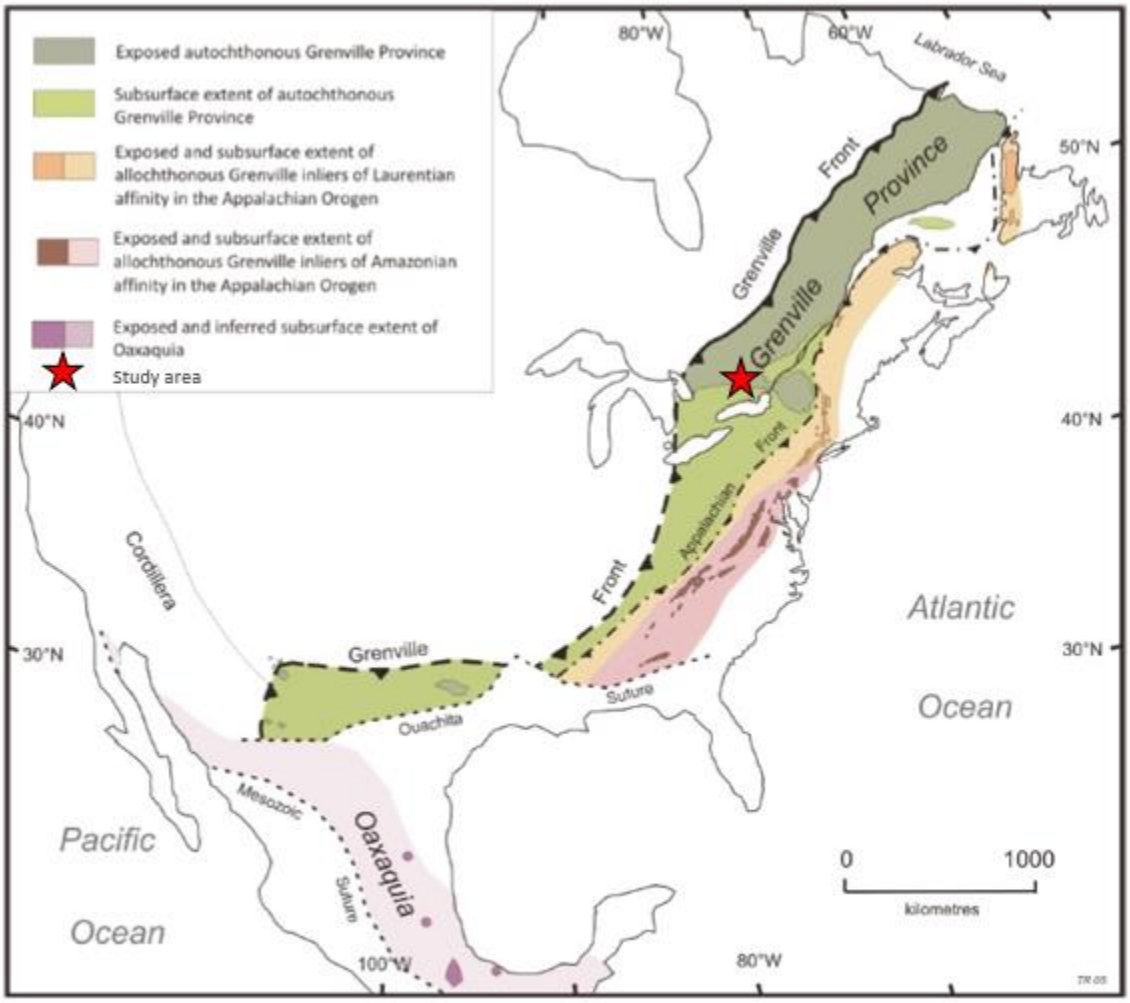

Figure 3.1. Lithotectonic divisions of the Grenville Province. Modified from Rivers et al. (2012).

In Canada, the southwestern Grenville Province is divided into three general lithotectonic segments; Laurentia (and its pre-Grenvillian margin), the Composite Arc Belt, and the Frontenac-Adirondack Belt (Figure 3.2) (Carr et al., 2000; Rivers et al., 2012). Laurentia and its margin include the exposures of the Archean Superior and Paleoproterozoic Southern Province rocks with 1800–1350 Ma supracrustal and continental Grenvillian arc rocks (Carr et al., 2000). The

Laurentain margin rocks can be separated into three levels (L1, L2, L3) based on their inferred structural levels during orogenesis (Figure 3.2). The Frontenac-Adirondack Belt is composed of 1300–1240 Ma and 1180–1155 Ma calc-alkaline arc rocks and 1130 Ma anorthosite (Carr et al., 2000). Lastly, the Composite Arc Belt is dominated by <1300 Ma volcanic, plutonic, volcaniclastic, siliciclastic, and carbonate rocks (Carr et al., 2000). Each of these segments is further divided by lithologic and isotopic affinities, deformation history, and inferred tectonic setting. The study site of this thesis (Bancroft Region) in found in the Composite Arc Belt.

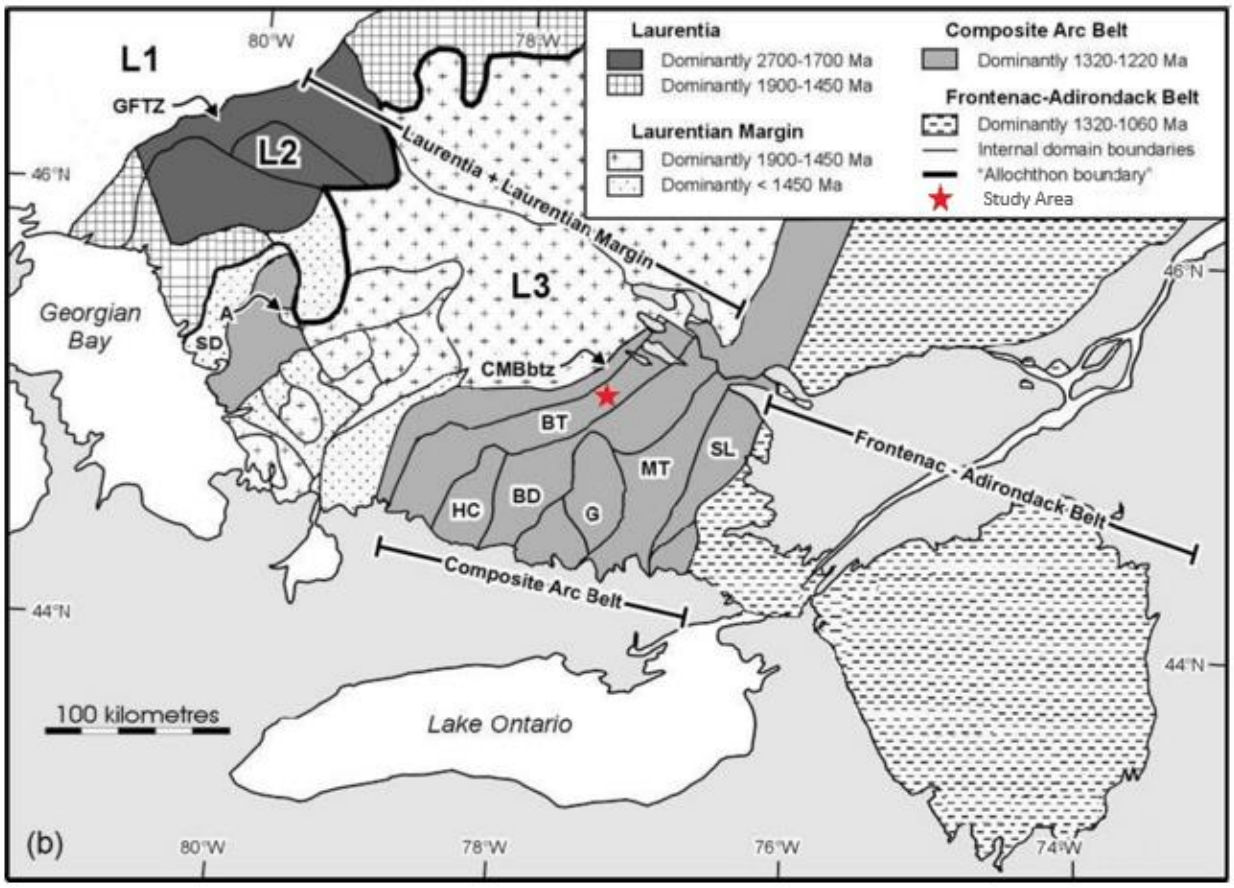

Figure 3.2. Southwestern Grenville Province subdivisions modified from Carr et al. (2000). Domains in the Composite Arc Belt are the Central Metasedimentary Belt boundary thrust zone (CMBbtz), the Harvey Cardiff Arch (HC), the Belmont domain (BD), the Grimsthorpe domain (G), the Mazinaw terrane (MT), the Sharbot Lake domain (SL), and the Bancroft terrane (BT).

3.2 Composite Arc Belt

The current exposure of the Composite Arc Belt extends from the Central Metasedimentary Belt boundary thrust zone in the northwest to the Maberly shear zone in the southeast (Figure 3.2). The primary tectonic environments recorded by the Composite Arc Belt are proposed to be arcs, rifted arcs, primitive arcs, and continental fragments, with associated carbonate and clastic sedimentary rocks (Carr et al., 2000). Between 1300 and 1250 Ma carbonate and clastic sediments were deposited with associated emplaced mafic and felsic volcanic rocks and tonalites (Carr et al., 2000). Multiple periods of magmatism occurred between 1280 and 1030 Ma where rocks were deformed and metamorphosed at (mostly) amphibolite-facies conditions during Grenville orogenesis (Carr et al., 2000). The Composite Arc Belt is divided into specific lithologic and magmatic associations representing elements of a larger arc system that was later amalgamated. The inferred boundaries of these domains are shown in Figure 3.2. Individual terranes and domains exhibit unique supracrustal successions, suggesting that they developed independently on different basement substrates (Carr et al., 2000).

3.3 Bancroft Terrane

The Bancroft terrane (BT) is bordered by the Central Metasedimentary Belt boundary thrust zone (CMBbtz) to the North-West and the Belmont domain (BD) and the Harvey-Cardiff Arch (HC) to the South-East (Rivers et al., 2012) (Figure 3.2). The CMBbtz is a northeast-southwest–trending thrust zone consisting of metaplutonic thrust sheets enveloped in gneissic tectonites and calcitic-dolomitic marble (Agustsson et al., 2013). The BD and HC are considered a part of the Elzevir Terrane and are underlain by a 1.3 Ga ophiolitic substrate; these terranes were proposed to have developed in a marginal back-arc basin tectonically assembled in an oceanic realm before accretion to Laurentia (Rivers et al., 2012).

The Bancroft Terrane (the focus of this thesis) has a tonalitic basement of the proposed continental-margin arc and is inferred to have developed in a platformal setting on the Laurentian margin (Rivers et al., 2012) as thrust sheets amalgamated onto the margin (Agustsson et al., 2013). It is characterized by the presence of middle to upper amphibolite-grade orthogneisses (Carlson et al., 1990), calcite marble, and clastic metasedimentary rocks (Sangster et al., 1992). It was intruded by a nepheline syenite suite (>1.22 Ga) (Miller, 1984) and a younger carbonatite/pegmatite suite (1.09–1.04 Ga; Heaman et al., 1988). The Bancroft Terrane contains carbonatites (Moecher et al., 1997) and calcite-rich rocks that may be pseudocarbonatites but are of unknown petrogenesis (Lentz 1998, 1999; Moyd, 1990).

4.0 Methods

4.1 Petrology and mineral compositions

Samples were processed at the University of Waterloo. Whole-rock samples collected from outcrops were cut into thick section billets using a rock saw. Polished thick sections were made and viewed under a petrographic microscope at the University of Waterloo. A petrological study was conducted to determine minerology and observe textures of the samples. Descriptions of mineral assemblages and microstructures yield information on determining rock type and ultimately petrogenesis.

A Leo 1530 scanning electron microscope (SEM) with energy dispersive x-ray spectroscopy (EDX) was used for mineral identification for two representative samples. The SEM provides detailed high-resolution images of the samples by detecting backscattered electron signals while the EDX is used to provide elemental identification and quantitative compositional information. Samples were coated with gold and analyzed using an operative voltage of 20 kV.

4.2 Trace element compositions

Calcite separates were obtained from whole-rock samples through crushing and hand picking under a binocular microscope. Approximately 10g of material was powdered in an agate mortar and pestle for each sample. Agate was chosen for its hardness so that there was minimal contamination of metals. The mortar and pestle were cleaned with ethanol between samples to minimize cross-contamination between samples.

Trace element concentrations were determined in calcite powders in the Metal Isotope and Geochemistry Laboratory at the University of Waterloo using Agilent 8800 QQQ-ICP-MS. Powdered samples were added to LPDE (low-density polyethylene) vials and dissolved in 1M HCl for 24 hours. An aliquot of the same was taken for an approximate dilution factor of 5000 for analysis by ICP-MS. After drying down, samples were dissolved in 10 mL of 1M HNO_3. Samples were dried down again and then dissolved further in 6 mL of 1M HNO_3 and topped up to 10 mL for analysis in He gas mode in the collision cell. Operating parameters for the Agilent 8800 QQQ-ICP-MS are summarized in table 4.1. Samples were added to the ICP-MS with standards, blanks, and washes. The ICP-MS was run with one wash between every five samples. An ASX-520 autosampler was used. Several secondary reference materials (USGS water samples T207, T211, T225, T231) were analyzed for assurance and quality control (Appendix A). Concentrations of trace elements K, V, Ba, Sr, Y, Pb and U are within 10% of their expected values. Several elements were within 15% of the accepted values (Co, Mo, Ni). For the REE, the LREE (La, Ce, Pr, Nd, Sm and Gd) were within 10% of the accepted values, but Dy and Er were within 20%. Average detection limits for each element are listed in Appendix B.

Table 4.1. Instrumental operating parameters for trace element ICP-MS analysis

Agilent Technologies 8800 ICP-MS Triple Quadrupole	
RF power	1550 W
RF matching	1.80 V
Sample cone	Nickel (x-lens)
Skimmer cone	Nickel (x-lens)
Sample depth	7.5 mm
Carrier gas	1.08 L min^{-1} (Ar)
Integration time	100 ms for 6 cycles
Masses measured	^{31}P, ^{39}K, ^{47}Ti, ^{51}V, ^{59}Co, ^{60}Ni, ^{85}Rb, ^{88}Sr, ^{89}Y, ^{90}Zr, ^{95}Mo, ^{137}Ba, ^{139}La, ^{140}Ce, ^{141}Pr, ^{146}Nd, ^{147}Sm, ^{153}Eu, ^{157}Gd, ^{159}Tb, ^{163}Dy, ^{165}Ho, ^{166}Er, ^{169}Er, ^{172}Yb, ^{175}Lu, ^{178}Hf, ^{185}Re, ^{208}Pb
Internal standards	^{45}Sc, ^{115}In, ^{209}Bi
Scan type	MS/MS (He gas; 3.6 mL/min)
Autosampler	ASX-520

4.3 Carbon and oxygen isotope analysis

The powdered calcite samples analyzed for trace elements were also analyzed for carbon and oxygen isotopic ratios at the Environmental Isotope Lab (EIL) at the University of Waterloo. Carbon and oxygen isotope ratios were determined by the production of carbon dioxide (CO_2) from carbonate minerals by reaction with 100% phosphoric acid (H_3PO_4) at 90^oC using a procedure based on the principles of Epstein et al. (1953). Samples and standards were weighed into 3.7 mL flat bottom Exetainer^{TM} septum vials, sealed, and then flushed with helium. 100% phosphoric acid was injected into the vial which was then placed in an aluminum tray maintained at 90 ± 0.1^oC for more than 1 hour. The CO_2 was extracted automatically with a double-hole needle Gilson auto-sampler connected to a GVI MultiFlow (IsoPrime MultiFlow User's Guide v1.1, 2014). The MultiFlow separates CO_2, N_2, O_2 and H_2O. The purified CO_2 travels into the GVI IsoPrime continuous flow isotope ratio mass spectrometer system (CF-IRMS) that measures the isotope ratios for carbon and oxygen (IsoPrime100 User's Guide v1.02 for Ionvantage, 2014). Quality control is maintained by including a variety of lab and international standards from the IAEA and NIST with duplicates run approximately every tenth sample. A minimum of 10% duplicate analysis were conducted. Results are recorded based on standard corrections which include the four calibrated standards, EIL-21 (traceable to NBS-18 and NBS-19) + IAEA-CO-1, IAEA-CO-8 and IAEA-CO-9 used for normalization. During a sample run, linearity checks are included using a suite of EIL-21 to produce a range of peak heights that encompass the expected sample peaks range.

Notation for the dataset is reported in terms of the per mil variation in isotope ratios relative to a standard (δ notation), defined by the following:

$$\delta\ (per\ mil) = \left[\frac{R_{sample}}{R_{standard}}\right] * 1000$$

Where R = $^{18}O/^{16}O$ or $^{13}C/^{12}C$, and the standard is VPDB (Vienna Pee Dee Belemnite). This is a standard identical to PDB (Pee Dee Belemnite) which was introduced by Craig (1957) when taken from a fossil of *Belemnitela americana* of the Cretaceous Pee Dee Formation in South Carolina. To compare these results with common rock types, the $\delta^{18}O$ values are calculated for VSMOW (Vienna Standard Mean Ocean Water). VSMOW is the current accepted standard for mean ocean water and was prepared by the International Atomic Energy Agency (IAEA) from distilled seawater. It is comparable to the first proposed standard by Craig (1961), SMOW (Standard Mean Ocean Water) that was calibrated relative to a sample from the Potomac River. The equation relating VSMOW and VPDB is as follows:

$$\delta^{18}O_{VSMOW} = 1.03091 * \delta^{18}O_{VPDB} + 30.91‰$$

4.4 Strontium isotope analysis

Powdered samples of calcite were sent to the Environmental Isotope Lab at the University of Waterloo for $^{87}Sr/^{86}Sr$ isotopic ratios. Purified and acid digested strontium was loaded on 1–2 zone refined degassed Re filaments and was ionized and analyzed for $^{87}Sr/^{86}Sr$ using a Thermo-Finnegan Triton thermal ionization mass spectrometer (TIMS). The results are calibrated by using the NIST-SRM-987 strontium carbonate isotopic standard ($^{87}Sr/^{86}Sr = 0.710245$ $2\sigma_x = 0.000015$) which also corrects for Rb interference.

A minimum of one in five samples was repeated to ensure repeatability. Sample precision is calculated using approximately 200 discrete measurements per sample. The variability of these measurements is used to calculate the precision. A 2σ less than ± 0.0003 and $2\sigma_x$ less than ± 0.000015 is acceptable.

5.0 Results

5.1 Field relationships

There are several carbonate-bearing rock types in the Bancroft region, including carbonatites, calcite-rich rocks (potential pseudocarbonatites), marbles, metadolostone, and nepheline syenites. Carbonatites and pseudocarbonatites are difficult to distinguish from one another in the field because of their similar mineral assemblages and textures. There are two dominant carbonate rock types in the study area: (1) marbles that have a conformable relationship with their host rocks, and (2) calcite-rich rocks that have an apparent intrusive relationship with their host rocks. Although hosted by different map units (Figure 5.1), the different carbonate rocks are petrologically similar in the field (i.e., similar grain sizes and mineral assemblages). Below are general descriptions of each rock type in outcrop and sample locations are found in Table 5.1. Detailed petrological descriptions of each rock type are found in section 5.2.

Samples were taken from roadside outcrops located in and around the Bancroft region (Figure 5.1; Table 5.1). Outcrops that were sampled had coarse-grained calcite in calcite-rich rocks, marble, metadolostone, or nepheline syenite. Samples are found in several different lithological fields defined by Sanford and Baer (1971). Most samples (19AM01, 19AM02/20AM07, 19AM05, 20AM01, 20AM02, 20AM06, 20AM08, 20AM09, 20AM10, 20AM11, 20AM12, 20AM14, 20AM15, and 20AM17) are found within biotitic quartzofeldspathic gneiss or hornblende-biotite gneiss map units. Samples 19AM04 and 20AM16 are found within the paragneiss region and samples 19AM03 and 20AM13 are found within the marble region. Samples 20AM03, 20AM04, and 20AM05 are found within the migmatite region from Sanford and Baer (1981). There is no apparent spatial pattern that distinguishes rock types from one another as seen in Figure 5.1.

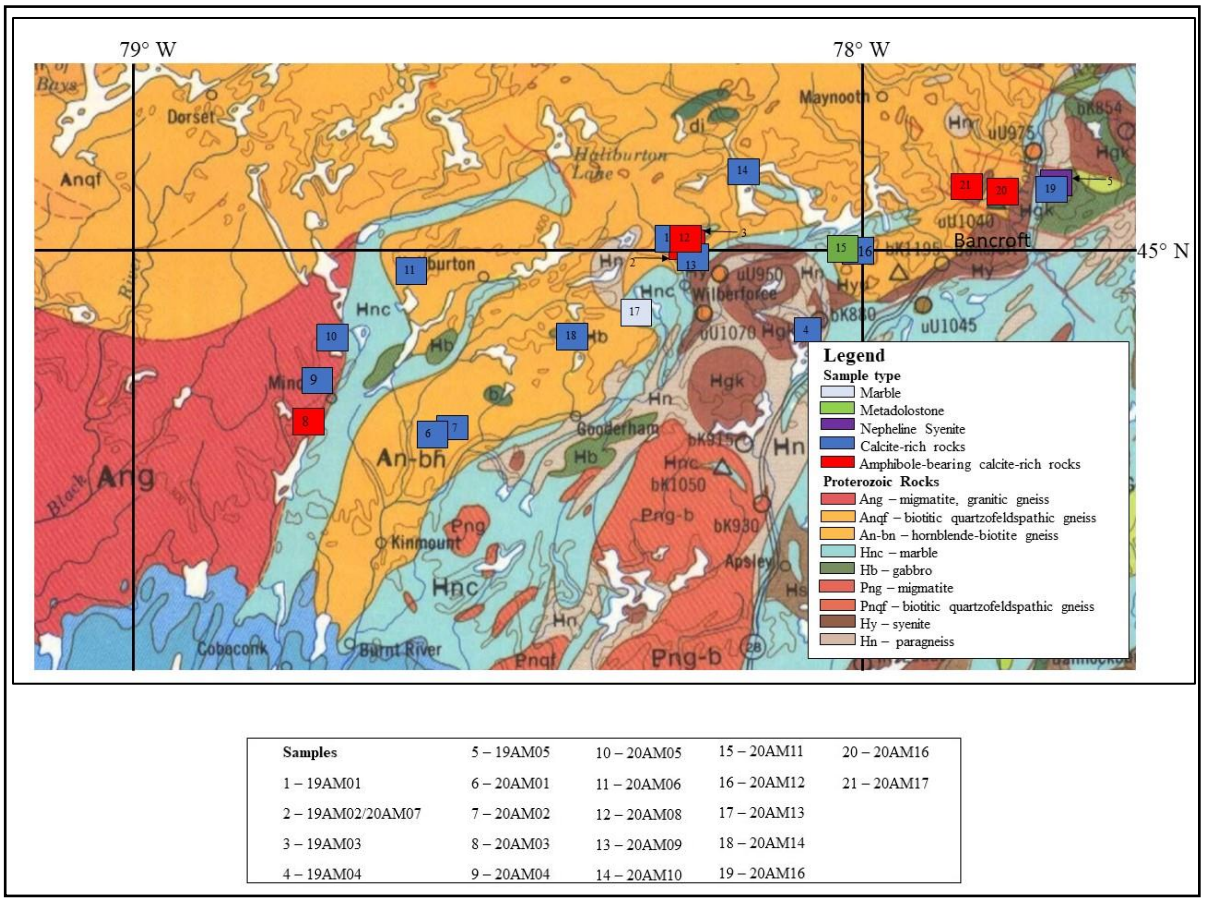

Samples	5 – 19AM05	10 – 20AM05	15 – 20AM11	20 – 20AM16
1 – 19AM01	6 – 20AM01	11 – 20AM06	16 – 20AM12	21 – 20AM17
2 – 19AM02/20AM07	7 – 20AM02	12 – 20AM08	17 – 20AM13	
3 – 19AM03	8 – 20AM03	13 – 20AM09	18 – 20AM14	
4 – 19AM04	9 – 20AM04	14 – 20AM10	19 – 20AM16	

Figure 5.1. Geologic Map of the Bancroft area modified from Sanford and Baer (1981) with sample locations.

Marble is found throughout the study region in multiple locations (sampling sites 19AM01, 19AM02, 19AM04, 20AM01, 20AM02, 20AM04, 20AM05, 20AM06, 20AM08, 20AM10, 20AM13, and 20AM14). Marble in outcrop can be up to 10m in thickness and can extend laterally for over 100m (Figure 5.2a). Marble has sharp contact boundaries with mafic host rocks (Figure 5.2b). In rare cases, marble shows local (meter-scale) skarn zones when intruded by pegmatite. Samples were collected from the core of large marbles to avoid the influence of skarn zones. Marble is biotite rich (Figure 5.2c) and has minor amounts of clinopyroxene, amphibole, and quartz (Table 5.3).

One sample (20AM11) is a homogeneous metadolostone (Figure 5.2d) and is found within a paragneiss unit. In outcrop, this rock type is distinct from marble by higher amounts of colourless mica (muscovite) and the abundance of dolomite.

Nepheline syenite in the Bancroft region contains cm-scale aggregates of calcite (Figure 5.2e). Samples were collected from a rock pit associated with nepheline syenite from a near-by quarry in the town of Bancroft and host other minerals such as biotite, sodalite, cancrinite, and zircon.

Calcite-rich rocks are divided into two groups: (1) calcite-rich rocks where carbonate (mainly calcite) is found in vein-like structures, and (2) calcite-rich rocks that are amphibole-bearing containing medium to coarse-grained amphibole. These groups are also distinguished by their calcite trace element concentrations (section 5.3).

Calcite-rich rocks without amphibole include samples from site 19AM04, 20AM01, 20AM02, 20AM04, 20AM05, 20AM06, 20AM09, 20AM10, 20AM12, 20AM14, and 20AM15. These calcite-rich rocks form veins up to 50cm in width (Figure 5.3a) with sharp contacts with the surrounding host rocks (Figure 5.3a). In outcrop, these rocks have moderate grain sizes (up to 5cm wide) and are generally homogeneous (Figure 5.3b), though some show colour gradation from pink to white at contact zones (Figure 5.3c).

The second group of calcite-rich rocks contain coarse grain amphibole up to 30cm wide (Figure 5.3d). These samples are found at locations 19AM02/20AM07, 19AM03, 20AM03, 20AM08, 20AM16, and 20AM17. The amphibole tends to be found with feldspar (Figure 5.3e) and on the outer edges of the calcite (Figure 5.3f). In outcrop, these rocks are homogeneous with similar grain sizes (up to 15cm) and mineral assemblages.

Table 5.1. Sample Descriptions

Sample #	Latitude	Longitude	Sample Site Description
19AM01	45.01323	78.26443	Homogeneous marble.
19AM02 A-F/ 20AM07 A-E	45.00958	78.25232	Massive coarse grain calcite in association with amphibole (richterite) and feldspar. Spatial association with marble.
19AM03	45.01170	78.24733	Coarse calcite vein-like structure containing coarse grain amphibole and phlogopite.
19AM04 A-C	44.91727	78.07702	Calcite vein-like structures throughout skarn.
19AM05 A-E	45.05736	77.85658	Minor amounts of calcite in nepheline syenite with biotite, feldspar, sodalite, cancrinite, and zircon.
	45.07007*	77.73244*	
20AM01 A-D	44.80810	78.59560	Calcite vein-like structure at contact between mafic and marble units.
20AM02 A-D	44.81660	78.57396	Calcite vein-like structures throughout foliated marble.
20AM03 A-I	44.82149	78.76573	Calcite vein-like structures crosscut through marble and mafic bodies. Calcite is associated with coarse feldspar and amphibole (richterite). Marble unit shows apophasis of calcite.
20AM04 A-B	44.86404	78.75966	Calcite is concentrated in vein-like structures that are associated with quartz, amphibole, and sulphides.
20AM05 A-C	44.90723	78.72916	Calcite found in mafic pods within layered marble unit.
20AM06 A-D	44.97864	78.62363	Coarse grain euhedral calcite is found associated with marble as well as within the mafic pods.
20AM08 A-I	45.01366	78.24282	Small calcite vein-like structures that crosscut or are associated with marble. Coarse grain feldspar and amphiboles associated with calcite.
20AM09 A-D	44.99037	78.22834	Calcite vein-like structures cut across felsic gneiss and marble. Calcite is concentrated in the foliations of the gneiss.
20AM10 A-C	45.08072	78.15764	Calcite vein-like structure at contact between marble and felsic units.
20AM11	45.00101	78.02873	Homogeneous metadolostone.
20AM12 A-D	45.00278	78.00587	Calcite pockets containing abundant coarse-grained apatite throughout marble and felsic units.
20AM13	44.93485	78.30765	Calcite vein-like structures throughout homogeneous marble outcrop.
20AM14 A-D	44.90799	78.38899	Coarse calcite at contact of marble and pegmatite units.
20AM15 A-B	45.06791	77.73013	Coarse calcite found concentrated in layers of layered marble.
20AM16 A-F	45.06654	77.79282	Cross-cutting calcite vein-like structures through pegmatite and mafic host. Calcite is in association with coarse grained feldspar and amphibole (richterite).
20AM17 A-C	45.06570	77.85416	Calcite found at contact between felsic and marble units with coarse amphibole (richterite) and sulphides.

*Indicates the location of the quarry site of the nepheline syenite.

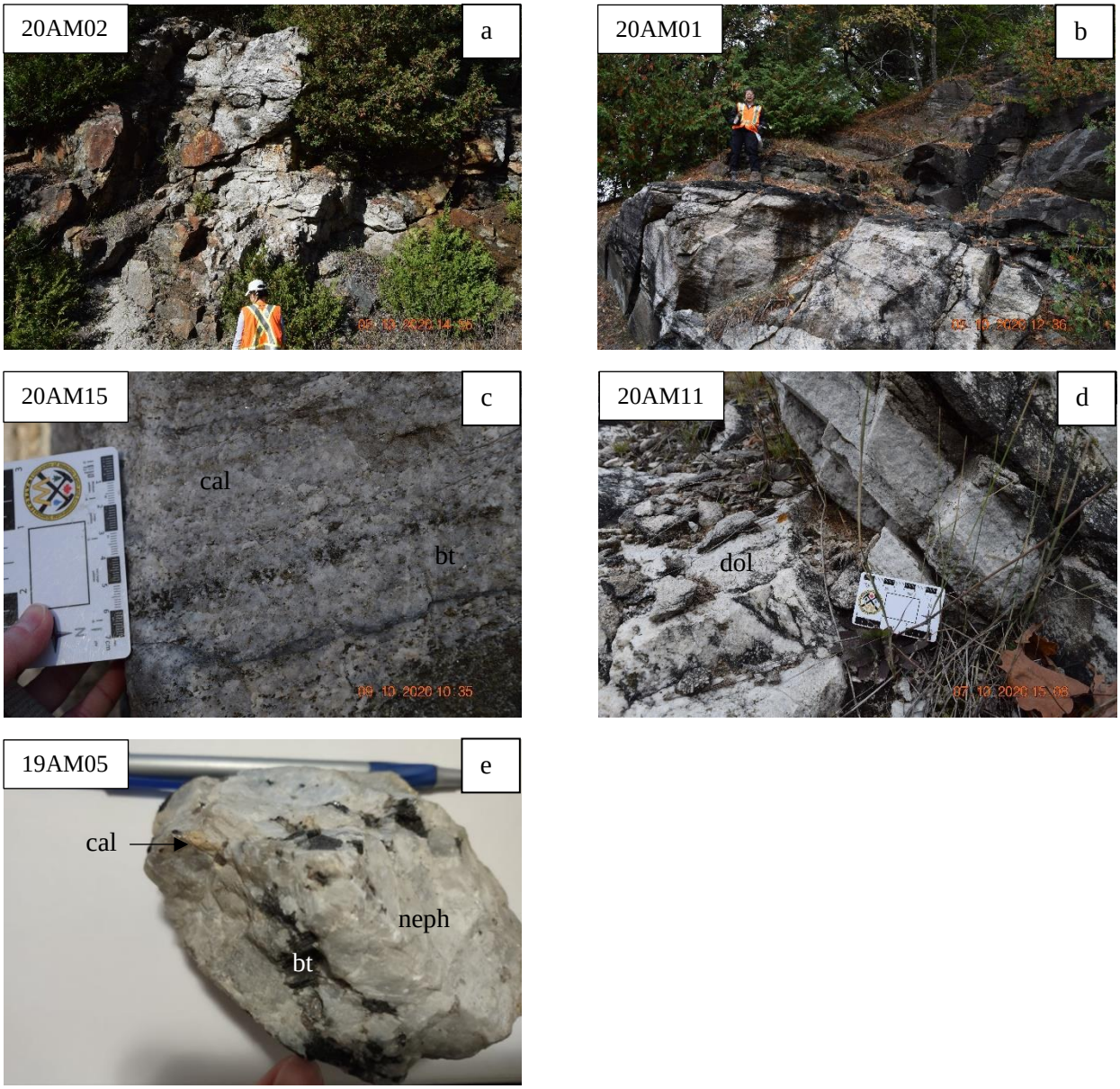

Figure 5.2. Outcrop photos of marble, metadolostone, and nepheline syenite. a) Homogeneous laterally extensive marble outcrop b) Marble outcrop with sharp contact boundary to mafic host rock. c) Close up of marble sample showing a mineral assemblage of mainly calcite and biotite. d) Close up of metadolostone showing a mineral assemblage of mainly dolomite. e) Grab sample of nepheline syenite with beige calcite and biotite.

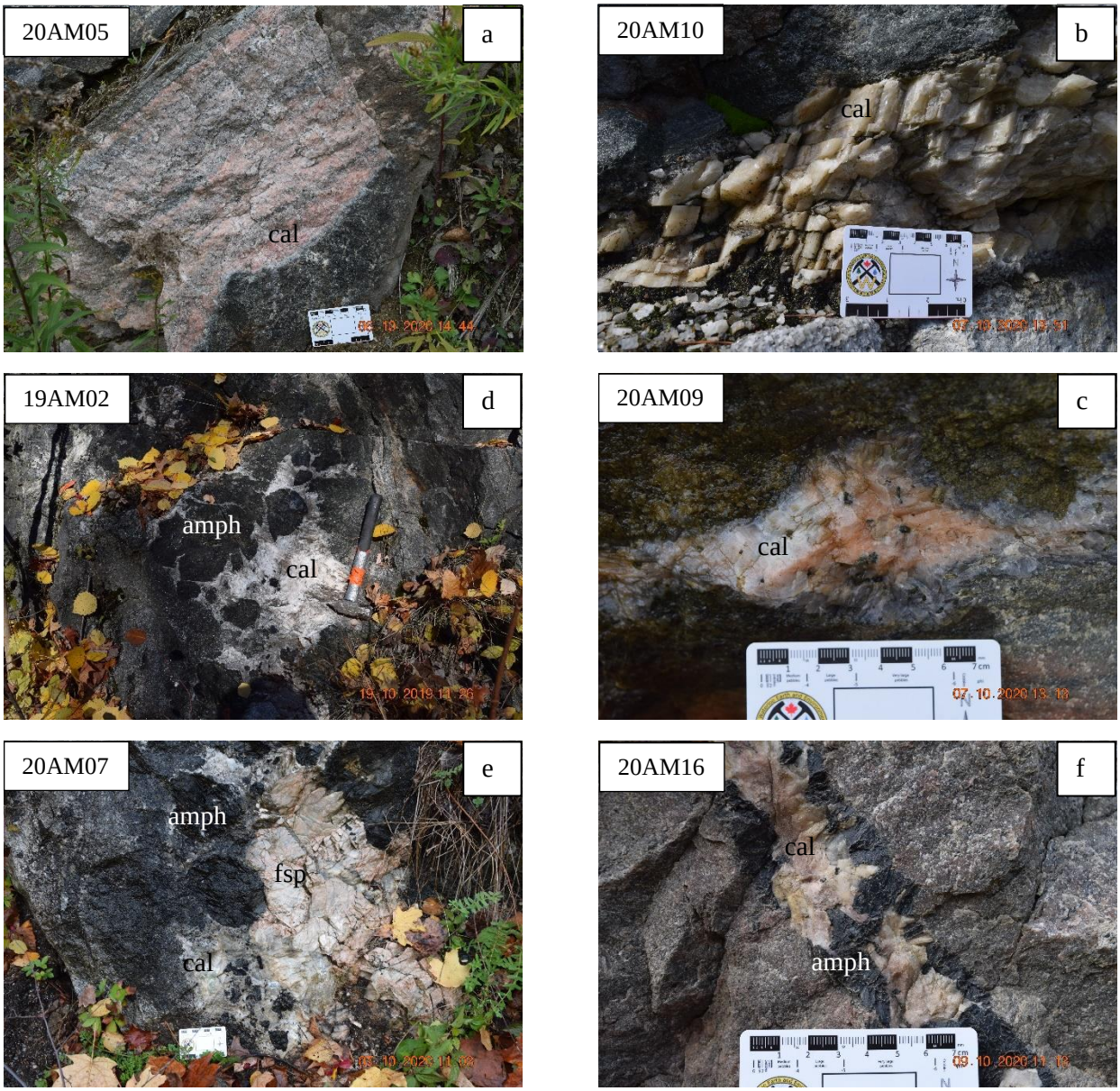

Figure 5.3. Outcrop photos of calcite-rich rocks. a) Wide vein-like structure of calcite-rich rock with sharp boundary to host rock. b) Coarse grain calcite in calcite-rich rock. c) Calcite transitioning colours from pink to white in calcite-rich rock. d) Calcite-rich rock with very coarse grain amphibole. e) Amphibole and feldspar contact in amphibole-bearing calcite-rich rock. f) Amphibole concentrated at the contact of the calcite-rich rock and host rock in amphibole-bearing calcite-rich rock.

5.2 Mineral assemblages and textures

Mineral assemblages and textures were identified in thick section using optical petrology for marble, metadolostone, nepheline syenite, calcite-rich rocks, and amphibole-bearing calcite-rich rocks and two representative samples were analyzed using SEM-EDX. A summary of mineral assemblages in each rock type is shown in Table 5.2. Measured mineral compositions for two representative samples from an amphibole-bearing and amphibole-absent calcite-rocks from SEM-EDX are shown in Table 5.2 and an example of a SEM-EDX spectrum is shown in Figure 5.4. All mineral proportions reported below are estimated volumetric proportions (vol.%).

Marble is coarse grained (usually 2–10 mm in grain sizes), equigranular, unfoliated, and generally homogeneous over meters to tens of meters. Samples are generally >70% calcite and >10% biotite with minor amounts of clinopyroxene (1–5%), amphibole (hornblende) (1–5%), quartz (1–5%), feldspar (plagioclase) (1–2%) and Fe-oxides (e.g., magnetite) (1–2%) (Figure 5.5a/b).

The metadolostone sample is coarse grained (1–5 mm in grain size), equigranular, and homogeneous over several meters. The sample contains >80% dolomite with minor amounts of muscovite (Figure 5.5c).

The nepheline syenite samples are found in a quarry site. The samples contain >60% coarse grained (1-10 mm in grain size), equigranular nepheline with coarse grain (1–10 mm in grain size) alkali feldspar (albite), biotite, cancrinite, and sodalite, with minor (<5%) coarse grained (1–5 mm in grain size) calcite and zircon (Figure 5.5d/e).

Calcite-rich rocks are separated into two groups, those that are amphibole-bearing and those that are not. These groups are also differentiated based on geochemistry (section 5.3 below). Both groups contain small amounts of clinopyroxene and biotite.

The amphibole-absent calcite-rich rocks are coarse grained (generally >5mm in grain size), equigranular, unfoliated, and homogeneous (Figure 5.6a). They contain >70% calcite with biotite that is Mg-rich, and forms disseminated flakes up to 5 mm in width. Clinopyroxene is Ca-rich and forms subhedral to euhedral grains up to 2mm in size (Figure 5.6b/c). These are interstitial along calcite grain boundaries and rarely found as inclusions in calcite. Titanite is subhedral to euhedral and up to 1mm in grain size.

The amphibole-bearing calcite-rich rocks are coarse grained (generally >5mm in grain size), equigranular, unfoliated, and heterogeneous (Figure 5.6d). They have >60% calcite with coarse grained amphibole (up to 30cm across) concentrated along the margins of the contact of calcite with the host rock. Amphibole is euhedral, does not contain any inclusions, and large crystals form clusters in some areas of the calcite rock whereas other portions contain no amphibole (Figure 5.6e). SEM-EDX measurement of a representative amphibole (Table 5.2) shows the composition is the richterite variety. Biotite is Mg-rich, and forms disseminated flakes up to 5 mm in width and clinopyroxene is Na-rich and forms subhedral to euhedral grains up to 2mm in size. Calcite can be found as inclusions in clinopyroxene, amphibole, and biotite (Figure 5.6f).

Table 5.2. Semi-quantitative composition of minerals from SEM-EDX

	19AM02F3				20AM09A			
Element (wt%)	Cal	Amp	Bt	Cpx	Cal	Ttn	Bt	Cpx
Si	bdl	28.4	23.5	27.7	bdl	14.4	20.5	25.0
Al	bdl	4.3	6.4	0.9	bdl	3.3	5.9	0.5
Mg	0.6	13.4	16.5	13.3	bdl	bdl	10.9	8.3
Fe	bdl	4.0	3.0	3.4	bdl	bdl	8.1	4.6
Ca	44.6	6.7	bdl	6.5	40.5	21.0	bdl	17.4
Na	bdl	3.5	bdl	3.7	bdl	bdl	bdl	bdl
K	bdl	1.4	10.4	1.3	bdl	bdl	8.0	bdl
F	bdl	bdl	bdl	bdl	bdl	bdl	bdl	bdl
T	bdl	bdl	bdl	bdl	bdl	18.4	bdl	bdl
O	44.6	41.1	40.3	43.2	45.7	39.3	38.4	39.4
C	12.2	bdl	bdl	bdl	13.8	3.6	8.3	4.9
Total	102.0	102.8	100.1	100.0	100.0	100.0	100.1	100.1

* bdl represents values below detection limits

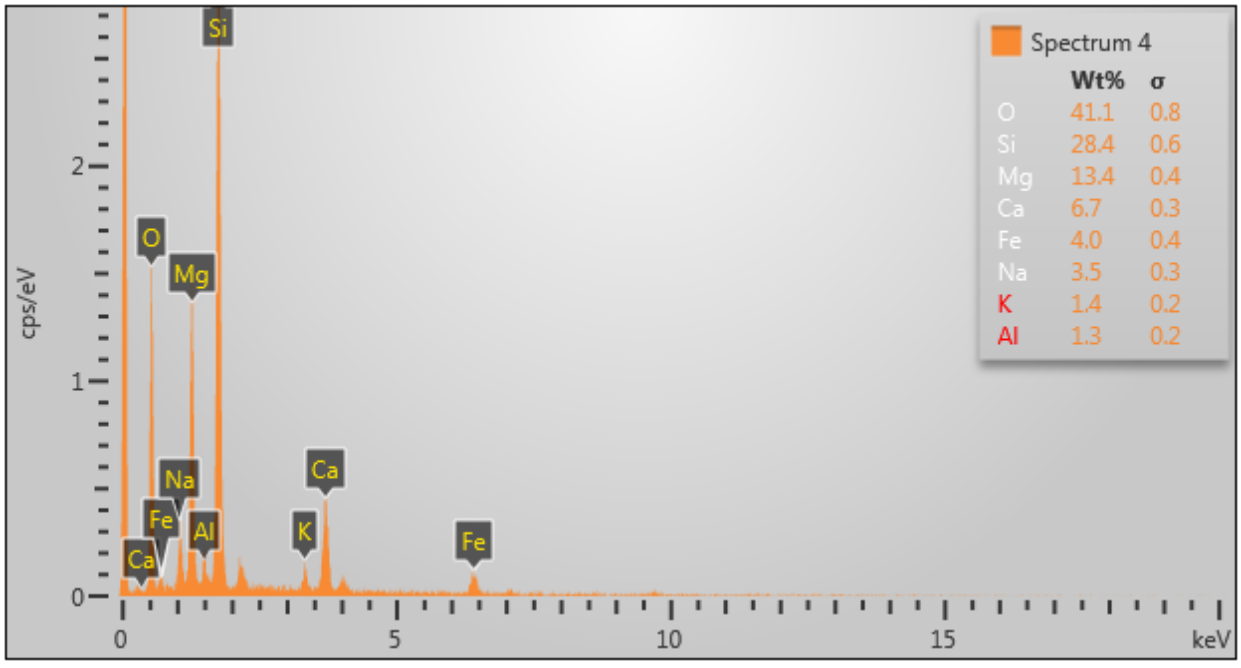

Figure 5.4. An example of EDS spectra (acquired with an SEM) for richterite from sample 19AM02F3.

Table 5.3. Mineral Assemblages

	Cal	Fsp	Bt	Qz	Cpx	Amp	Dol	Ms	Nph	Ttn
Marble										
19AM01A	X	X	X	X						
19AM02C	X		X		X	X				
19AM02D1	X		X							
19AM02D2	X		X		X	X				
19AM04A	X		X	X						
20AM02D	X		X							
20AM04B	X		X		X					
20AM05A	X		X		X					
20AM05B	X				X					
20AM10C	X									
20AM13A	X									
20AM14B	X		X							
Metadolostone										
20AM11A							X	X		
Nepheline syenite										
19AM05A	X	X	X						X	
19AM05B	X	X	X						X	
19AM05C	X	X	X						X	
Calcite-rich rocks										
19AM02E	X		X		X	X				
19AM02F	X		X		X	X				
19AM03A	X		X		X	X				
19AM04B1	X		X		X					
19AM04C	X		X							
20AM01B	X		X		X					
20AM05C	X									
20AM09A	X		X		X					X
20AM09B	X		X		X					X
20AM09C	X		X		X					X
20AM10A	X		X		X					

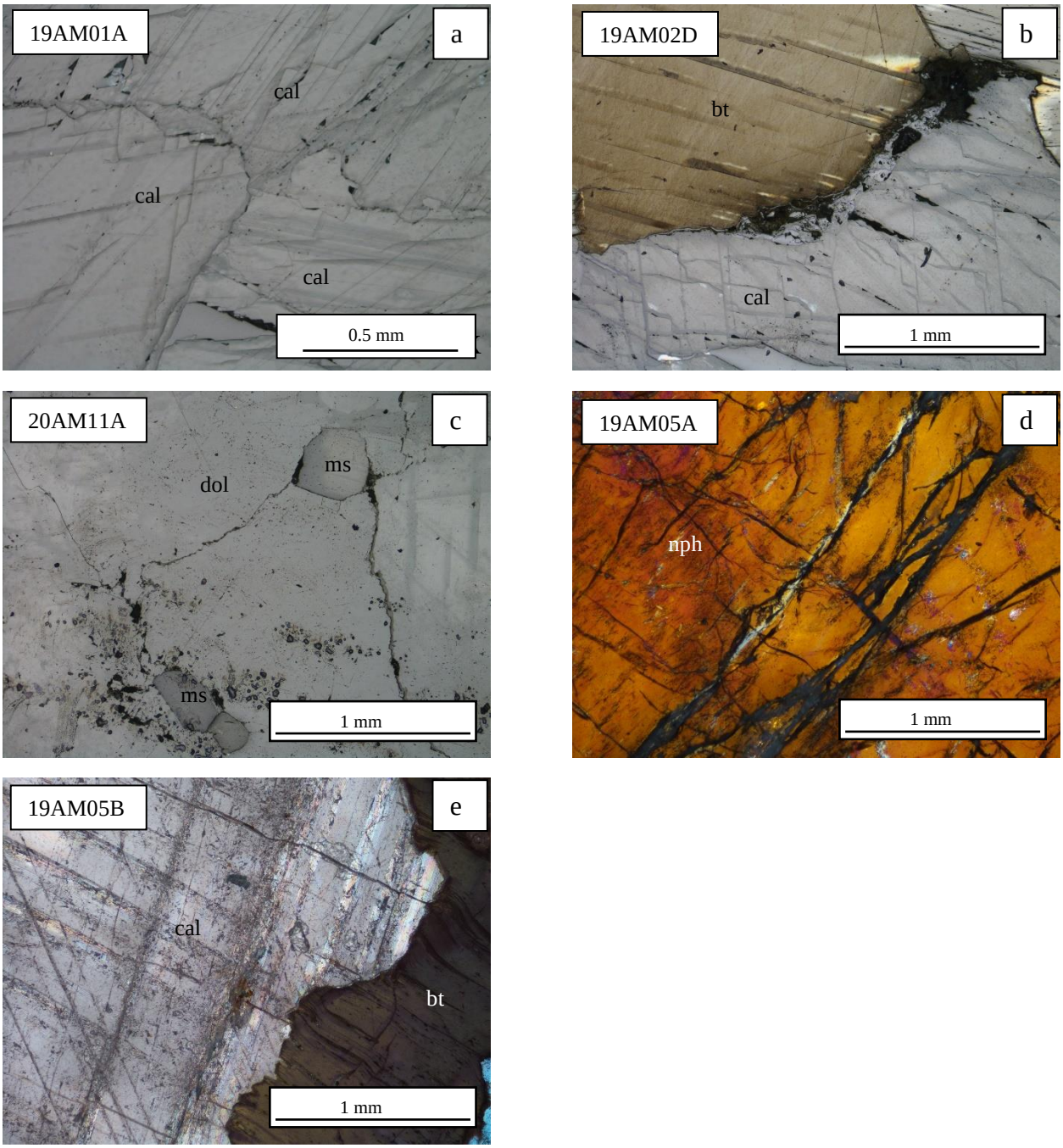

Figure 5.5. Thick section photos of marble, metadolostone, and nepheline syenite. a) Equigranular calcite grains in marble under plane polarized light. b) Massive biotite and calcite in marble under plane polarized light. c) Muscovite and dolomite in metadolostone under plane polarized light. d) Massive nepheline in nepheline syenite under cross polarized light. e) Massive biotite and calcite in nepheline syenite under cross polarized light.

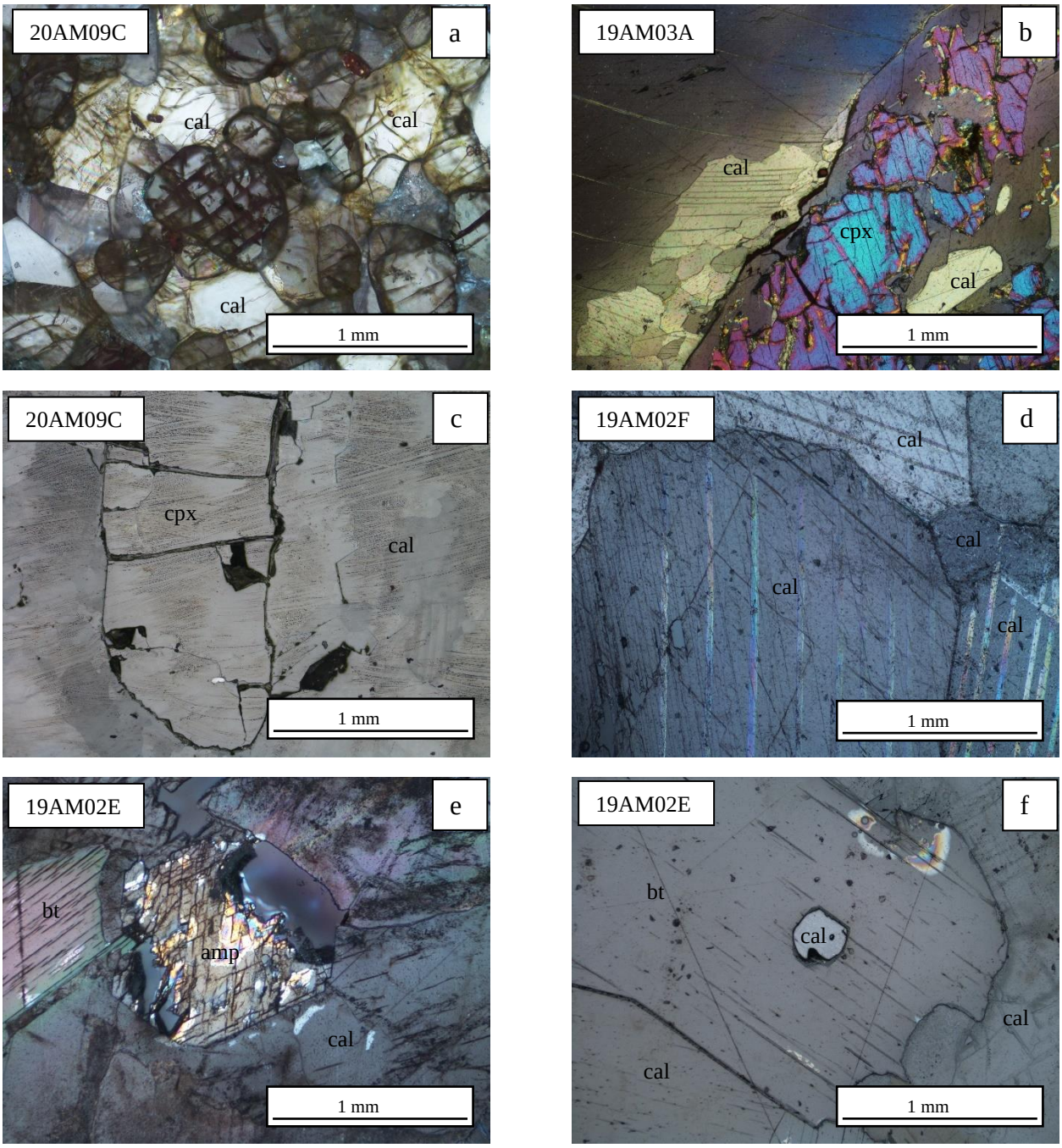

Figure 5.6. Thick section photos of calcite-rich rocks. a) Equigranular calcite in calcite-rich rock under cross polarized light. b) Clinopyroxene and calcite in calcite-rich rock under cross polarized light. c) Clinopyroxene and calcite in calcite-rich rock under plane polarized light. d) Equigranular calcite in amphibole-bearing calcite-rich rock under cross polarized light. e) Amphibole and biotite in amphibole-bearing calcite-rich rock under cross polarized light. f) Calcite inclusion in biotite in amphibole-bearing calcite-rich rocks under plane polarized light.

5.3 REE geochemistry

Concentrations of REE in calcite vary within and between the different lithological sample groups. Based on the compositional results described below, marbles, amphibole-bearing calcite-rich rocks, and calcite-rich rocks are each divided into multiple subgroups based on chondrite-normalized (see Appendix C) REE patterns. Concentrations of trace elements in calcite are reported in Table 5.4. Marbles are divided into two groups, amphibole-absent calcite-rich rocks into three groups, amphibole-bearing calcite-rich rocks into two groups, and metadolostone and calcite in nepheline syenite are treated separately below.

5.3.1 Marbles

The first group of marbles (marbles group 1) (n = 7) is defined by relatively high concentrations of LREE and HREE, with La concentrations over 60 ppm and Lu concentrations over 0.62 ppm (excluding sample 20AM01C). Chondrite-normalized REE patterns for this group have steep slopes with La_n/Lu_n values that range from 7.6–80.0. This group has relatively flat chondrite-normalized HREE Gd_n/Yb_n ratios of 1.7–3.3 and steep La_n/Sm_n ratios of 2.3–21.2. Eu anomalies for this group are weak to absent with Eu/Eu* (where $Eu/Eu^* = Eu_n/(Sm_n * Gd_n)^{0.5}$) varying from 0.6–1.2. One sample has a bell-shaped REE pattern (Sample 20AM01C, Figure 5.7a). In general, the concentrations and patterns of chondrite-normalized REE do not align with the reported Bancroft marble values (Mungall, 1989) (Figure 5.7a).

The second group of marbles (marbles group 2) (n = 10) is defined by low concentrations of LREE values with La concentrations under 45 ppm and very low HREE concentrations with Lu values under 0.11 ppm. Chondrite-normalized REE patterns for this group have moderate slopes with La_n/Lu_n ratios of 0.7–20.2. This group has relatively flat chondrite-normalized HREE and LREE patterns with Gd_n/Yb_n ratios of 2.0–5.7 and La_n/Sm_n ratios of 0.1–5.9. Eu anomalies for this

group are weak to absent with Eu/Eu* varying from 0.6–1.0. In general, the concentrations and patterns of chondrite-normalized REE are similar to marbles from the Bancroft area reported by Mungall (1989) (Figure 5.7a).

5.3.2 Metadolostone

The metadolostone group consists of one sample (20AM11A) and is defined by low LREE concentrations and very low HREE concentrations with a La concentration of 1.93 ppm and an Lu concentration of 0.01 ppm. The chondrite-normalized REE pattern for this group has a steep slope with a La_n/Lu_n value of 36.3. This group has relatively gentle chondrite-normalized HREE and LREE slopes with a Gd_n/Yb_n ratio of 4.0 and a La_n/Sm_n ratio of 5.8. The Eu anomaly for this group is weak with an Eu/Eu* of 0.8 (Figure 5.7b).

5.3.3 Nepheline syenite

Calcite from nepheline syenite (n = 3) are defined by high LREE and HREE concentrations with La values over 150 ppm and Lu values over 3.0 ppm. Chondrite-normalized REE patterns for this group have gentle slopes with La_n/Lu_n values that range from 4.2–6.1. This group has relatively flat chondrite-normalized HREE Gd_n/Yb_n ratios of 0.9–1.0 and La_n/Sm_n ratios of 3.9–5.1. Eu anomalies for this group are weak with Eu/Eu* varying from 0.7–0.8. These samples have patterns and concentrations similar samples of nepheline syenite from the Grenville Province in Western Quebec (Breemen and Currie, 2004) (Figure 5.7b).

5.3.4 Calcite-rich rocks

The first group (group 1) of amphibole-absent calcite-rich rocks (n = 9) have high LREE values with La concentrations over 15 ppm and low HREE values with Lu concentrations under 0.3 ppm. Chondrite-normalized REE patterns for this group have steep slopes with La_n/Lu_n values that range from 6.1–49.5. This group has relatively steep chondrite-normalized LREE slopes with

La_n/Sm_n ratios of 3.9–19.7 and gentle HREE slopes with Gd_n/Yb_n ratios of 1.4–4.5. Eu anomalies for this group are weak to absent with Eu/Eu* varying from 0.6–1.0. All samples have lower values of chondrite-normalized REE than carbonatites from Bancroft reported by Mungall (1989) and carbonatites from Grenville reported by Moecher et al. (1997) (Figure 5.8a).

The second group (group 2) of amphibole-absent calcite-rich rocks (n = 5) are defined by high LREE and HREE values with La concentrations over 21 ppm and Lu concentrations over 0.5 ppm. Chondrite-normalized REE patterns for this group have gentle slopes with La_n/Lu_n values that range from 3.9–12.3. This group has relatively gentle chondrite-normalized LREE slopes with La_n/Sm_n ratios of 3.5–7.2 and absent HREE slopes with Gd_n/Yb_n ratios of 0.8–1.6. Eu anomalies for this group are weak to absent with Eu/Eu* varying from 0.5–0.8. Samples have similar concentrations to Bancroft carbonatites reported by Mungall (1989) and carbonatites from Grenville reported by Moecher et al. (1997), however they have differing REE patterns and slopes (Figure 5.8b).

The final group (group 3) of amphibole-absent calcite-rich rocks (n = 6) have REE concentrations and patterns that do not fit into the previously defined calcite-rich rocks group 1 and 2 (Figure 5.8c).

Sample 20AM06C and 20AM01B differ from calcite-rich rocks group 1 and 2 because they have very low La_n/Sm_n ratios of 1.2–1.3. These samples also have moderate to high La_n/Lu_n and Gd_n/Yb_n ratios ranging from 6.3–21.9 and 3.2-11.3 respectively.

Samples 20AM06A and 20AM06B differ from calcite-rich rocks Group 1 and 2 because they have a bell shape REE with La concentrations of 15.9–18.5 ppm and Lu concentrations of

0.64–0.90 ppm. The La_n/Lu_n are low and range from 2.2–2.7. The La_n/Sm_n and Gd_n/Yb_n ratios are also low ranging from 0.2–0.3 and 5.7–7.4 respectively.

Sample 20AM02A has a La_n/Lu_n ratio of 2.8 which is lower than samples from calcite-rich rocks group 1 and 2; the La_n/Sm_n ratio is 1.6 which is also lower than the La_n/Sm_n ratio for calcite-rich rocks group 1 and 2 while the Gd_n/Yb_n ratio is 1.6.

Sample 20AM10A has very low LREE values with a La concentration of 0.36 ppm and higher HREE values with a Lu concentration of 0.96 ppm. This gives sample 20AM10A a positively sloping chondrite-normalized REE slope pattern while all other calcite-rich rocks have a flat or negatively sloping chondrite-normalized REE pattern. The Eu/Eu* ratio of this sample is 0.5 and the La_n/Lu_n, La_n/Sm_n, and Gd_n/Yb_n ratios are low with values of 0.04, 0.3, and 0.3 respectively.

5.3.5 Amphibole-bearing calcite-rich rocks

Amphibole-bearing calcite-rich rocks group 1 (n = 6) is defined by high LREE values with La concentrations over 265 ppm. Chondrite-normalized REE patterns for this group have moderate to high slopes with La_n/Lu_n values that range from 7.0–33.1. This group has relatively flat chondrite-normalized HREE and LREE patterns with Gd_n/Yb_n ratios of 1.0–2.4 and La_n/Sm_n ratios of 3.6–10.3. Eu anomalies for this group are weak with Eu/Eu* varying from 0.4–0.7. In general, the patterns of chondrite-normalized REE from amphibole-bearing calcite-rich rocks group 1 are similar to carbonatites from the Bancroft area reported by Mungall (1989) and carbonatites from the Grenville Province reported by Moecher et al. (1997). However, the REE concentrations from amphibole-bearing calcite-rich rocks group 1 tend to be higher than those of these carbonatites; exceptions are samples 20AM08F and 20AM08B which plot in the compositional range of carbonatites from Mungall (1989) (Figure 5.9a).

Amphibole-bearing calcite-rich rocks group 2 (n = 5) is defined by lower LREE values with La concentrations under 195 ppm. Chondrite-normalized REE patterns for this group have U-shaped patterns with La_n/Lu_n values that range from 0.8–6.4. Gd_n/Yb_n ratios vary from 0.4–1.3 and La_n/Sm_n ratios from 1.4–6.5. Eu anomalies for this group are weak with Eu/Eu* varying from 0.7–0.8. In general, the concentrations of LREE from amphibole-bearing calcite-rich rocks group 2 are similar to carbonatites from the Bancroft area reported by Mungall (1989). However, the chondrite-normalized REE patterns are different with relative enrichment of HREE in amphibole-bearing calcite-rich rocks group 2 compared with the carbonatites (Figure 5.9b).

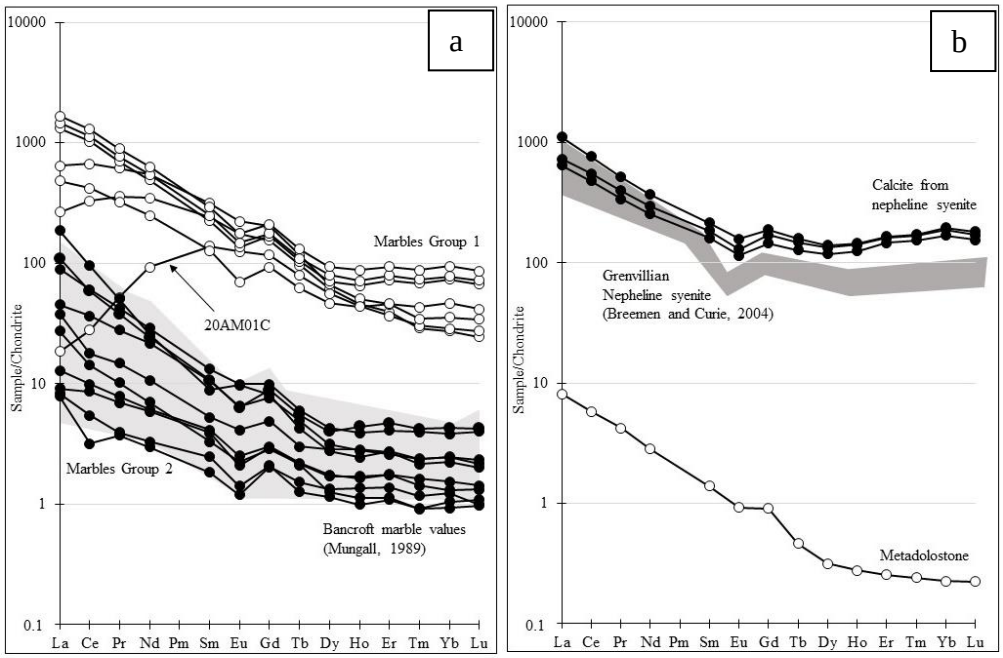

Figure 5.7. Chondrite-normalized rare earth element plots for calcite from marble, nepheline syenite, and metadolostone. a) Closed symbols represent marbles group 2 with lower REE concentrations while open symbols represent marbles group 1 with higher REE concentrations. The shaded area shows marble data from Mungall (1989). Sample 20AM01C is a bell-shaped sample that does not follow a typical marble trend. b) Closed symbols represent calcite from nepheline syenite samples and open symbols represent calcite from the metadolostone sample. The shaded region represents nepheline syenite data from the Grenville Province region in Western Quebec from Breemen and Currie (2004). Chondrite values are from McDonough and Sun (1995) and can be found in Appendix C.

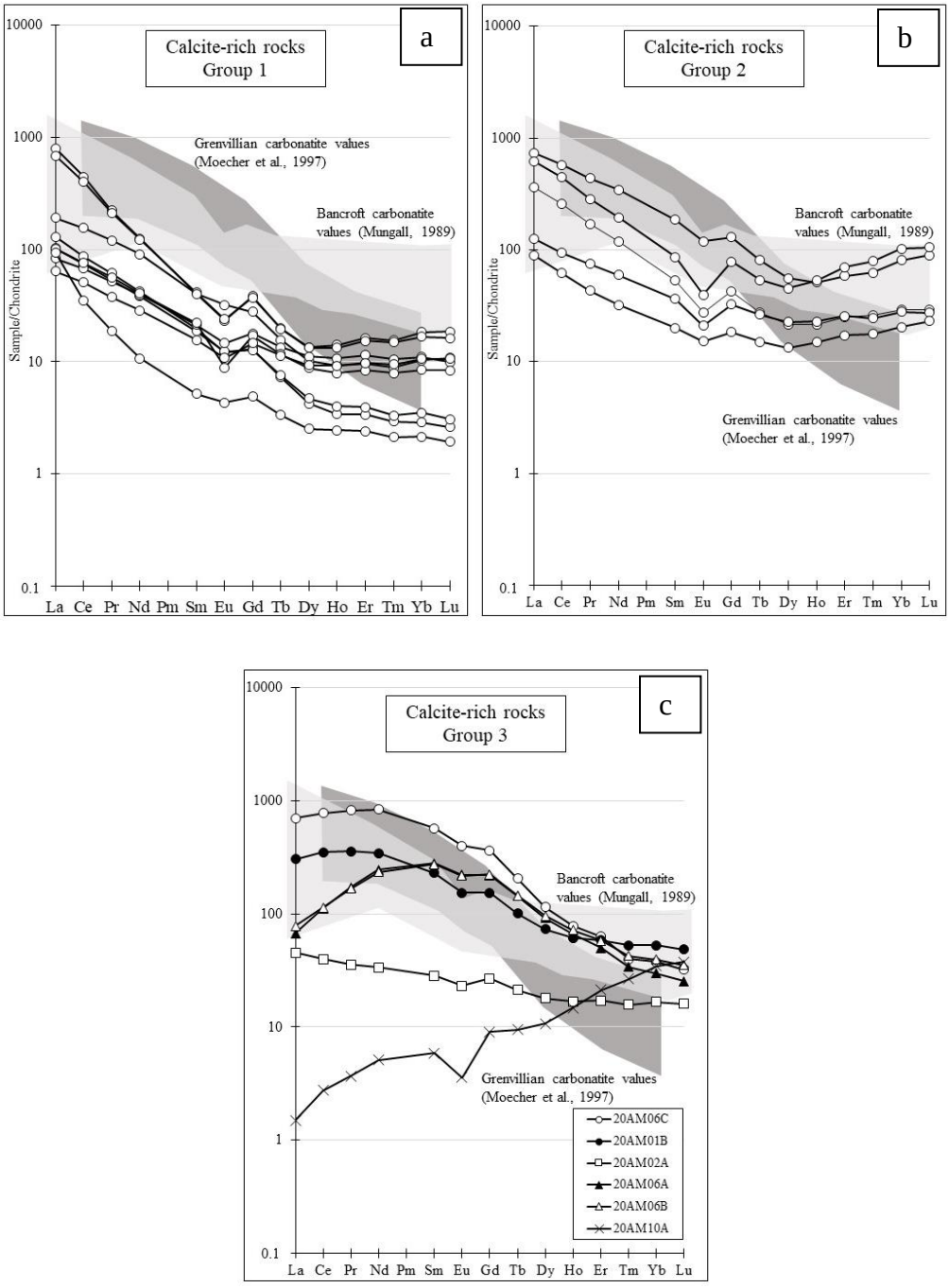

Figure 5.8. Chondrite-normalized rare earth element plots for calcite-rich rocks. The light shaded area represents Bancroft carbonatites from Mungall (1989) and the dark shaded area represents Grenvillian carbonatites from Moecher et al. (1997). a) Calcite-rich rocks group 1 contains samples with low HREE and higher Gd_n/Lu_n values. b) Calcite-rich rocks group 2 contains samples with high HREE and lower Gd_n/Lu_n values. c) Calcite-rich rocks group 3 contains samples that do not fit trends defined by group 1 or group 2. Chondrite values are from McDonough and Sun (1995) and can be found in Appendix C.

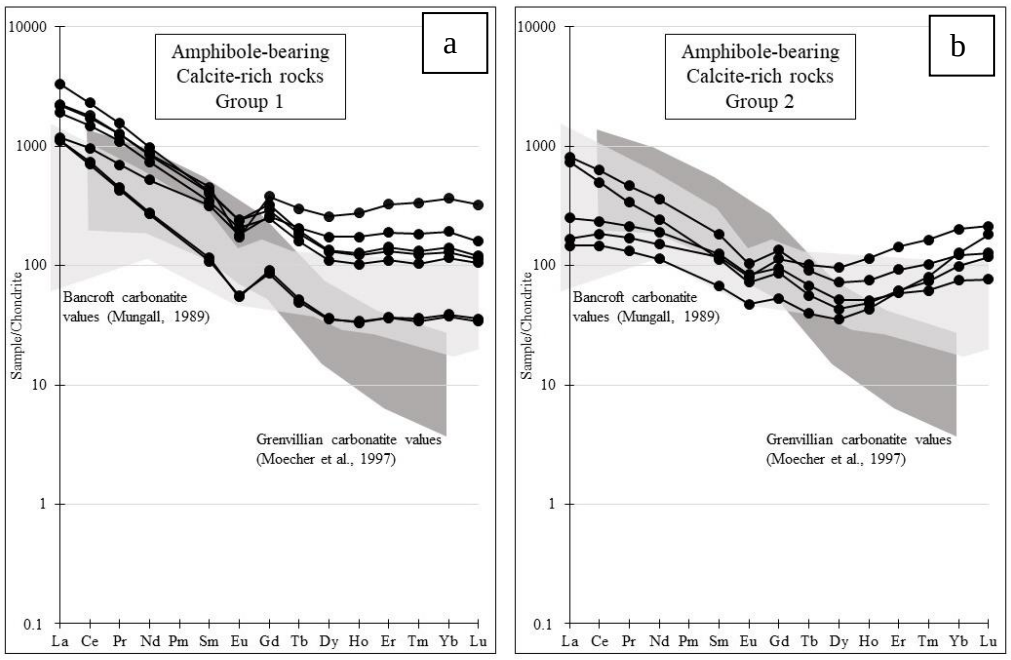

Figure 5.9. Chondrite-normalized rare earth element distribution plots for amphibole-bearing calcite-rich rocks. The light shaded area represents Bancroft carbonatites from Mungall (1989) and the dark shaded area represents Grenvillian carbonatites from Moecher et al. (1997). a) Amphibole-bearing calcite-rich rocks group 1 contains samples with higher LREE values. b) Amphibole-bearing calcite-rich rocks group 2 contains samples with lower LREE values. Chondrite values are from McDonough and Sun (1995) and can be found in Appendix C.

5.4 Trace element geochemistry

Measured concentrations of trace elements (along with REE) are presented in Table 5.4. The large ion lithophile elements (LILE) are of particular interest in carbonates considering their substitution for Ca^{2+} in calcite and dolomite. Concentrations of strontium (Sr), potassium (K), and barium (Ba) distinguish the various groups of the samples in this study. In general, samples enriched in Sr are also enriched in Ba (Figure 5.10).

Marbles group 1 (n = 7) have high concentrations of Sr ranging from 2730–7630 ppm and moderate concentrations of K ranging from 20.8–357 ppm. Ba concentrations are high ranging from 24.7–186 ppm (Figure 5.10).

Marbles group 2 (n = 10) have lower concentrations of Sr ranging from 108–1420 ppm and high concentrations of K ranging from 27.0–1270 ppm. Ba concentrations are low ranging from 0.21-37.7 ppm (Figure 5.10).

The metadolostone group (n = 1) has a very low concentration of Sr (55.4 ppm) and a moderate concentration of K (85.5 ppm). The Ba concentration is relatively low with a value of 32.0 ppm (Figure 5.10).

The nepheline syenites group (n = 3) have moderate concentrations of Sr ranging from 2370–2740 ppm and variable, but generally high concentrations of K ranging from 51.1–849 ppm. Ba concentrations are moderate ranging from 57.5–94.7 ppm (Figure 5.10). This group also has the highest thorium (Th) concentrations ranging from 0.31–15.2 ppm and the only group with detectable concentrations of zirconium (Zr) ranging from 1.33–3.22 ppm.

Calcite-rich rocks group 1 (n = 9) have moderate concentrations of Sr ranging from 421–3100 ppm and low concentrations of K ranging from 20.6–82.2 ppm. Ba concentrations are moderate ranging from 3.18–108 ppm (Figure 5.10).

Calcite-rich rocks group 2 (n = 5) have moderate concentrations of Sr ranging from 686–3270 ppm and low concentrations of K ranging from 19.4–45.2 ppm. Ba concentrations are moderate ranging from 2.11–149 ppm (Figure 5.10).

Calcite-rich rocks group 3 (n = 6) have very high concentrations of Sr ranging from 734–8200 ppm and low concentrations of K ranging from 26.7–46.7 ppm. Ba concentrations are low ranging from 1.25–43.1 ppm (Figure 5.10).

Amphibole-bearing calcite-rich rocks group 1 (n = 6) have high concentrations of Sr ranging from 2260–6670 ppm and low concentrations of K ranging from 26.1–57.4 ppm. Ba concentrations are high ranging from 34.1–332 ppm (Figure 5.10).

Amphibole-bearing calcite-rich rocks group 2 (n = 5) have high concentrations of Sr ranging from 1450–6720 ppm and moderate concentrations of K ranging from 26.8–81.1 ppm. Ba concentrations are moderate ranging from 20.7–151 ppm (Figure 5.10).

Table 5.4: Trace element compositions of calcite from various groups

	Marbles Group 1						
Sample	19AM02C	19AM02D1	19AM02D2	20AM01A	20AM01C	20AM06D	20AM08H
P (ppm)	67.6	bdl	39.0	7610	5120	7890	70.0
K	357	159	96.3	24.1	52.0	20.8	33.5
Ti	6.05	bdl	bdl	4.23	12.2	2.72	bdl
V	0.13	0.11	0.05	0.22	0.30	0.36	0.04
Co	0.11	0.15	0.13	0.99	0.27	0.83	0.06
Ni	0.49	1.28	0.58	0.67	0.47	0.75	0.86
Rb	1.29	0.59	0.22	0.11	0.14	bdl	bdl
Sr	3210	3530	3190	4320	7630	6740	2730
Y	118	125	151	66.8	71.2	85.4	78.9
Zr	bdl	bdl	bdl	bdl	bdl	bdl	bdl
Mo	bdl	bdl	bdl	bdl	bdl	bdl	bdl
Ba	157	165	186	68.5	52.5	24.7	51.9
La	313	346	396	63.1	4.39	153	115
Ce	628	690	796	203	17.1	408	257
Pr	65.2	71.3	83.0	33.1	4.82	56.8	29.9
Nd	226	248	290	160	42.4	250	114
Sm	33.3	37.0	43.1	35.8	20.5	46.6	18.9
Eu	7.63	8.35	9.95	9.91	7.01	12.5	3.93
Gd	33.4	35.1	42.0	30.8	23.3	40.2	18.5
Tb	3.74	3.94	4.75	3.46	2.86	4.19	2.25
Dy	17.4	19.7	22.9	15.1	13.8	16.5	11.5
Ho	3.57	3.92	4.77	2.53	2.42	2.76	2.38
Er	11.6	12.6	15.0	6.28	5.85	7.34	7.38
Tm	1.68	1.82	2.18	0.72	0.75	0.85	1.07
Yb	11.8	12.6	15.3	4.39	4.64	5.75	7.48
Lu	1.70	1.84	2.19	0.62	0.69	0.87	1.06
Hf	bdl	bdl	bdl	bdl	bdl	bdl	bdl
W	bdl	bdl	bdl	bdl	bdl	bdl	bdl
Re	0.02	0.02	0.03	0.01	0.02	0.01	0.02
Pb	21.0	24.4	25.5	3.53	8.45	16.0	5.61
Th	bdl	0.14	bdl	0.55	0.34	1.28	bdl
U	bdl	bdl	bdl	0.27	0.26	1.03	bdl

Table 5.4. *continued*

	Marbles Group 2						
Sample	19AM01A	19AM04A	20AM02D	20AM04B	20AM05A	20AM05B	20AM08I
P (ppm)	41.0	bdl	139	70.7	188	52.4	143
K	48.5	1270	138	27.0	85.1	45.8	35.0
Ti	bdl	25.1	5.24	bdl	1.94	1.89	bdl
V	0.40	3.02	0.63	0.11	0.26	0.16	0.06
Co	0.28	bdl	0.24	0.09	0.08	0.29	0.05
Ni	1.19	bdl	1.63	0.63	0.70	0.80	0.73
Rb	bdl	1.23	1.14	bdl	0.35	bdl	bdl
Sr	881	108	387	1220	636	188	1420
Y	4.6	1.75	2.89	7.35	8.47	3.46	4.12
Zr	bdl	bdl	bdl	bdl	bdl	bdl	bdl
Mo	bdl	bdl	bdl	bdl	bdl	bdl	bdl
Ba	37.7	28.8	0.55	14.9	8.71	23.7	26.9
La	10.8	1.97	3.06	21.1	26.0	6.51	44.4
Ce	22.3	3.34	6.10	36.9	36.0	8.73	58.7
Pr	2.60	0.37	0.73	3.94	3.50	0.95	4.70
Nd	9.88	1.51	2.80	13.3	11.0	3.20	11.9
Sm	1.57	0.37	0.61	1.96	1.58	0.49	1.31
Eu	0.37	0.08	0.14	0.56	0.36	0.13	0.55
Gd	1.52	0.42	0.60	1.98	1.77	0.57	1.62
Tb	0.18	0.05	0.08	0.22	0.20	0.08	0.15
Dy	0.78	0.28	0.43	1.05	0.98	0.42	0.68
Ho	0.15	0.05	0.09	0.21	0.24	0.09	0.13
Er	0.42	0.17	0.28	0.65	0.75	0.28	0.44
Tm	0.06	0.02	0.04	0.10	0.10	0.04	0.06
Yb	0.40	0.17	0.25	0.62	0.69	0.21	0.39
Lu	0.06	0.03	0.04	0.10	0.11	0.03	0.06
Hf	bdl	bdl	bdl	bdl	bdl	bdl	bdl
W	bdl	bdl	bdl	bdl	bdl	bdl	bdl
Re	0.01	0.05	0.01	0.02	0.01	0.02	0.02
Pb	6.59	5.24	1.63	6.25	1.91	5.07	3.20
Th	0.64	bdl	bdl	bdl	bdl	bdl	bdl
U	0.11	bdl	bdl	0.14	0.03	bdl	0.05

Table 5.4. *continued*

	Marbles Group 2 Cnt.			Metadolostone	Nepheline Syenite		
Sample	20AM10C	20AM13A	20AM14B	20AM11A	NEPH SY 01	NEPH SY 02	NEPH SY 03
P (ppm)	113	268	111	55.3	46.5	43.1	84.2
K	44.2	40.1	79.7	85.5	51.1	849	390
Ti	bdl	bdl	bdl	bdl	bdl	bdl	bdl
V	bdl	0.24	0.59	1.67	bdl	bdl	0.04
Co	0.07	0.16	0.24	0.06	0.30	0.20	0.16
Ni	0.77	0.89	1.41	0.57	0.56	0.46	0.63
Rb	bdl	bdl	bdl	bdl	0.13	1.89	0.26
Sr	532	376	641	137	2560	2740	2370
Y	2.10	3.20	6.26	0.50	232	257	258
Zr	bdl	bdl	bdl	bdl	bdl	3.22	1.33
Mo	bdl	bdl	bdl	bdl	bdl	bdl	bdl
Ba	0.21	12.3	31.2	32.0	89.3	94.7	57.5
La	2.16	1.86	9.00	1.93	154	262	173
Ce	5.26	1.96	11.0	3.55	294	467	338
Pr	0.64	0.35	1.37	0.39	31.6	48.1	36.9
Nd	2.69	1.36	4.87	1.30	116	168	135
Sm	0.58	0.27	0.78	0.21	23.9	31.9	27.5
Eu	0.12	0.07	0.23	0.05	6.47	8.89	7.32
Gd	0.59	0.41	0.97	0.18	29.0	37.4	33.9
Tb	0.08	0.06	0.11	0.02	4.60	5.74	5.36
Dy	0.31	0.33	0.70	0.08	29.1	34.5	33.0
Ho	0.06	0.07	0.16	0.02	6.86	7.95	7.72
Er	0.18	0.22	0.43	0.04	23.5	26.6	25.7
Tm	0.02	0.03	0.05	0.01	3.80	4.26	4.17
Yb	0.15	0.20	0.36	0.04	27.1	31.4	30.3
Lu	0.02	0.03	0.05	0.01	3.94	4.61	4.33
Hf	bdl	bdl	bdl	bdl	bdl	bdl	bdl
W	bdl	bdl	bdl	bdl	bdl	0.35	bdl
Re	0.01	0.01	0.02	0.02	0.04	0.05	0.05
Pb	0.18	3.01	7.5	2.64	75.8	82.3	69.5
Th	bdl	bdl	bdl	bdl	0.31	15.21	4.45
U	0.2	0.05	0.04	0.12	0.11	3.87	0.19

Table 5.4. *continued*

	Calcite-rich Rocks Group 1						
Sample	19AM04B	19AM04C	20AM03F	20AM04A	20AM09A	20AM09B	20AM09C
P (ppm)	49.3	40.7	149	51.2	41.4	47.4	44.2
K	60.1	82.2	22.2	20.6	33.6	36.9	42.9
Ti	bdl	bdl	bdl	bdl	bdl	bdl	bdl
V	0.03	bdl	0.14	bdl	bdl	bdl	bdl
Co	0.12	0.11	0.08	0.24	0.12	0.11	0.16
Ni	0.69	0.72	0.67	0.66	0.81	0.72	0.76
Rb	bdl	bdl	bdl	bdl	bdl	bdl	bdl
Sr	1830	1660	1540	3100	588	421	496
Y	26.9	25.4	5.88	17.4	19.7	14.7	18.1
Zr	bdl	bdl	bdl	bdl	bdl	bdl	bdl
Mo	bdl	bdl	bdl	bdl	bdl	bdl	bdl
Ba	80.7	80.6	21.3	14.0	3.18	10.7	3.89
La	190	164	30.8	45.4	19.7	24.2	15.2
Ce	272	245	53.3	95.8	41.6	46.7	31.2
Pr	20.8	19.7	5.70	11.2	4.81	5.28	3.50
Nd	57.3	56.1	19.3	41.5	18.1	18.6	13.1
Sm	6.03	6.12	2.90	5.96	3.18	3.28	2.33
Eu	1.31	1.35	0.69	1.80	0.82	0.50	0.61
Gd	7.68	7.47	2.61	5.56	3.57	3.38	2.91
Tb	0.72	0.71	0.26	0.57	0.49	0.42	0.41
Dy	3.32	3.29	1.04	2.50	2.74	2.17	2.29
Ho	0.77	0.73	0.19	0.51	0.59	0.43	0.51
Er	2.59	2.46	0.54	1.55	1.84	1.34	1.56
Tm	0.38	0.37	0.07	0.22	0.26	0.20	0.23
Yb	2.97	2.69	0.46	1.66	1.78	1.37	1.71
Lu	0.47	0.41	0.07	0.27	0.25	0.21	0.27
Hf	bdl	bdl	bdl	bdl	bdl	bdl	bdl
W	bdl	bdl	bdl	bdl	bdl	bdl	bdl
Re	0.01	0.01	0.01	0.01	0.02	0.02	0.02
Pb	25.5	19.7	9.99	8.41	9.57	6.79	6.94
Th	0.98	0.31	0.16	bdl	bdl	bdl	bdl
U	0.04	0.03	bdl	bdl	bdl	bdl	bdl

Table 5.4. *continued*

	Calcite-rich Rocks Group 1 Cnt.		Calcite-rich Rocks Group 2				
Sample	20AM12D	20AM14A	20AM01D	20AM03E	20AM05C	20AM10B	20AM15B
P (ppm)	bdl	69.0	bdl	7630	61.9	93.1	56.4
K	44.2	67.4	bdl	19.4	36.8	32.0	45.2
Ti	bdl	bdl	bdl	5.54	bdl	bdl	bdl
V	bdl	bdl	bdl	0.63	0.05	bdl	0.04
Co	0.07	0.09	0.15	0.95	0.11	0.24	0.25
Ni	0.68	0.9	0.68	0.88	0.67	0.81	0.79
Rb	bdl	0.25	bdl	0.15	bdl	bdl	bdl
Sr	642	523	1740	3270	1320	1690	686
Y	6.67	5.49	26.3	97.9	41.2	142	40.3
Zr	bdl	bdl	bdl	bdl	bdl	bdl	bdl
Mo	bdl	bdl	bdl	bdl	bdl	bdl	bdl
Ba	108	20.8	2.11	149	17.8	16.5	6.31
La	24.4	22.3	21.3	174	85.3	147	29.7
Ce	45.0	21.4	37.8	351	157	273	57.2
Pr	4.98	1.75	3.98	40.6	15.9	26.5	6.92
Nd	17.6	4.89	14.7	157	53.9	89.2	27.2
Sm	2.76	0.77	2.97	27.5	7.89	12.8	5.36
Eu	0.70	0.24	0.85	6.68	1.56	2.23	1.18
Gd	2.54	0.98	3.65	25.9	8.42	15.6	6.47
Tb	0.27	0.12	0.54	2.90	0.98	1.93	0.95
Dy	1.16	0.62	3.26	13.7	5.29	11.1	5.56
Ho	0.22	0.13	0.81	2.78	1.18	2.91	1.24
Er	0.63	0.39	2.75	9.31	4.01	11.2	4.10
Tm	0.08	0.05	0.44	1.54	0.64	1.96	0.60
Yb	0.56	0.35	3.29	12.9	4.66	16.4	4.47
Lu	0.08	0.05	0.58	2.27	0.74	2.66	0.69
Hf	bdl	bdl	bdl	bdl	bdl	bdl	bdl
W	bdl	bdl	bdl	bdl	bdl	bdl	bdl
Re	0.02	0.01	0.02	0.02	0.02	0.03	0.01
Pb	20.3	14.1	3.06	12.7	9.36	6.47	2.69
Th	1.55	bdl	bdl	0.73	bdl	bdl	bdl
U	0.43	bdl	bdl	0.50	bdl	0.11	bdl

Table 5.4. *continued*

	Calcite-rich Rocks Group 3						Amphibole-bearing Clacite-rich Rocks Group 1
Sample	20AM01B	20AM02A	20AM06A	20AM06B	20AM06C	20AM10A	19AM02E
P (ppm)	5750	bdl	234	178	329	40.6	104
K	30.8	bdl	46.7	28.1	26.71	38.8	55.3
Ti	5.04	bdl	bdl	bdl	bdl	bdl	bdl
V	0.22	0.13	bdl	0.03	0.03	bdl	bdl
Co	0.50	0.17	0.54	0.57	1.07	0.23	0.27
Ni	0.54	0.73	0.79	0.87	0.75	0.87	0.83
Rb	0.19	bdl	0.1	0.09	bdl	bdl	bdl
Sr	4950	885	6330	5870	8200	734	6670
Y	95.0	27.2	103	123	126	41.4	224
Zr	bdl	bdl	bdl	bdl	bdl	bdl	bdl
Mo	bdl	bdl	bdl	bdl	bdl	bdl	bdl
Ba	11.8	8.58	14.4	22.2	43.1	1.25	332
La	72.1	10.8	15.9	18.5	167	0.36	523
Ce	214	24.5	68.6	69.5	477	1.68	1060
Pr	33.2	3.32	15.9	15.5	76.1	0.34	118
Nd	157	15.3	112	108	383	2.33	389
Sm	34.0	4.19	41.4	40.6	84.2	0.87	59.9
Eu	8.62	1.31	12.5	12.3	22.6	0.20	13.6
Gd	30.6	5.34	43.5	44.5	72.3	1.80	58.3
Tb	3.64	0.77	5.20	5.27	7.42	0.34	6.64
Dy	18.0	4.39	22.6	23.6	28.2	2.63	32.3
Ho	3.35	0.92	3.61	3.94	4.28	0.80	6.71
Er	9.34	2.73	7.97	9.23	10.1	3.39	21.2
Tm	1.30	0.39	0.84	1.05	0.99	0.66	3.07
Yb	8.51	2.68	4.77	6.34	6.05	5.58	20.9
Lu	1.23	0.41	0.64	0.90	0.82	0.96	2.91
Hf	bdl	bdl	bdl	bdl	bdl	bdl	bdl
W	bdl	bdl	bdl	bdl	bdl	bdl	bdl
Re	0.02	0.02	0.01	0.01	0.01	0.01	0.04
Pb	9.26	12.9	9.12	8.38	13.4	1.13	38.8
Th	1.88	bdl	bdl	0.14	0.24	bdl	0.36
U	0.57	bdl	0.04	0.06	0.06	bdl	0.03

Table 5.4. *continued*

	Amphibole-bearing Calcite-rich Rocks Group 1 Cnt.					Amphibole-bearing Calcite-rich Rocks Group 2	
Sample	19AM02F	19AM03A	20AM08B	20AM08F	20AM16F	20AM03A	20AM03B
P (ppm)	62.6	110	68.7	62.8	55.6	73.9	103
K	51.6	57.4	26.1	28.6	49.9	45.5	30.7
Ti	bdl	bdl	bdl	bdl	bdl	bdl	bdl
V	0.04	bdl	bdl	bdl	bdl	0.07	bdl
Co	0.13	0.11	0.06	0.06	0.15	0.18	0.21
Ni	0.70	0.82	0.64	0.73	0.56	0.71	0.66
Rb	0.09	bdl	bdl	bdl	0.13	0.39	bdl
Sr	5460	6510	2260	2340	4280	6470	5590
Y	190	248	62.9	66.8	302	95.6	150
Zr	bdl	bdl	bdl	bdl	bdl	bdl	bdl
Mo	bdl	bdl	bdl	bdl	bdl	bdl	bdl
Ba	265	181	69.6	34.1	213	151	49.8
La	453	795	269	267	281	176	194
Ce	915	1420	455	435	593	306	388
Pr	102	144	41.7	39.8	65.1	31.5	43.6
Nd	338	448	128	123	239	111	165
Sm	51.0	61.6	17.2	16.1	46.9	16.8	26.9
Eu	11.7	13.5	3.07	3.17	10.2	4.09	5.82
Gd	50.2	64.6	18.1	17.1	51.9	17.3	26.9
Tb	5.76	7.05	1.89	1.78	7.47	2.03	3.30
Dy	27.4	33.2	8.92	8.76	42.9	10.6	17.9
Ho	5.61	7.00	1.82	1.86	9.47	2.64	4.11
Er	17.7	22.8	5.84	5.92	30.2	9.87	14.9
Tm	2.58	3.29	0.85	0.90	4.55	1.83	2.55
Yb	18.7	22.8	6.06	6.26	31.0	16.0	19.8
Lu	2.68	3.06	0.87	0.91	4.05	3.02	3.25
Hf	bdl	bdl	bdl	bdl	bdl	bdl	bdl
W	bdl	bdl	bdl	bdl	0.38	bdl	bdl
Re	0.03	0.04	0.02	0.02	0.06	0.02	0.03
Pb	36.0	31.6	6.16	3.47	35.9	14.9	5.38
Th	0.31	1.00	bdl	bdl	bdl	bdl	bdl
U	0.04	0.15	0.04	0.55	0.06	0.08	0.63

Table 5.4. *continued*

	Amphibole-bearing Calcite-rich Rocks Group 2 Cnt.		
Sample	20AM03C	20AM03H	20AM16A
P (ppm)	1360	bdl	83.8
K	81.1	26.9	54.1
Ti	bdl	bdl	bdl
V	0.12	bdl	0.06
Co	0.30	0.14	0.67
Ni	0.76	0.69	0.53
Rb	0.82	bdl	0.13
Sr	5550	6720	1450
Y	98.3	82.7	271
Zr	bdl	bdl	bdl
Mo	bdl	bdl	bdl
Ba	84.4	89.3	20.7
La	59.6	34.8	39.6
Ce	145	90.4	113
Pr	19.9	12.3	15.9
Nd	87.7	52.2	69.3
Sm	18.6	9.94	17.3
Eu	4.75	2.67	4.52
Gd	19.0	10.6	22.7
Tb	2.45	1.44	3.68
Dy	12.7	8.71	23.8
Ho	2.80	2.37	6.26
Er	9.47	9.84	23.2
Tm	1.53	2.00	4.05
Yb	12.2	20.6	32.6
Lu	1.96	4.64	5.43
Hf	bdl	bdl	bdl
W	bdl	bdl	bdl
Re	0.02	0.03	0.05
Pb	5.91	6.18	6.92
Th	bdl	bdl	bdl
U	1.36	bdl	0.17

*bdl represents ‘below detection limit’. Detection limits for each element are located in Appendix B.

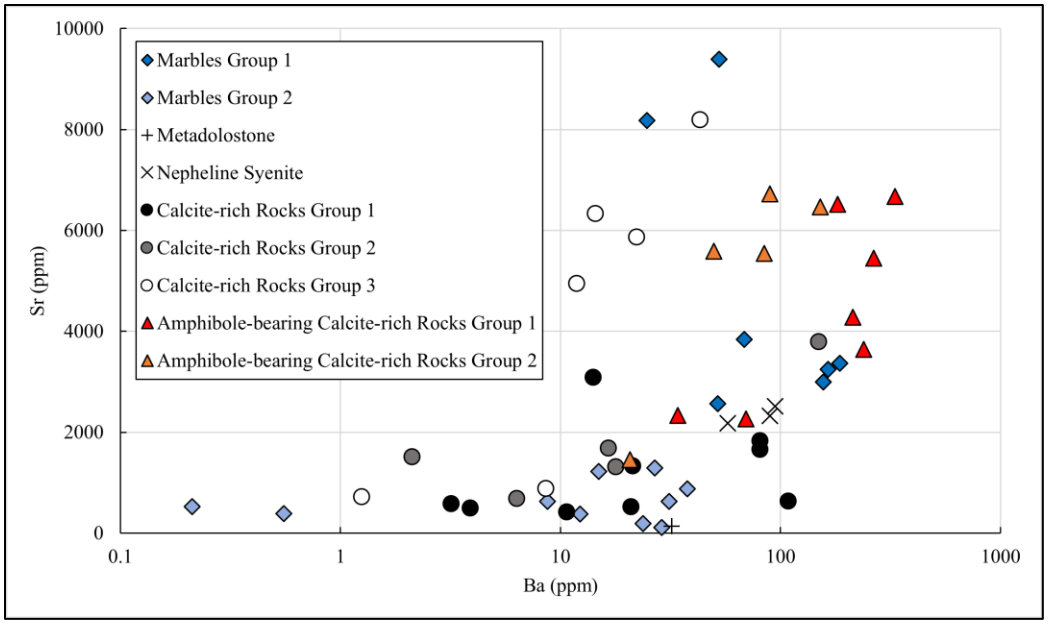

Figure 5.10. Barium and Strontium concentrations (ppm). Note that the amphibole-bearing calcite-rich rocks are generally enriched in Ba relative to the amphibole-absent calcite-rich rocks.

5.4 Carbon and oxygen isotope analysis

Oxygen and carbon stable isotopes values are shown presented Table 5.5 and Figure 5.11. Groups are determined by rare earth element patterns and are compared against different limestone and carbonatite groups from the literature (Bell and Simonetti, 2010).

Marbles group 1 (n = 7) have $\delta^{13}C_{PDB}$ and $\delta^{18}O_{VSMOW}$ values that range from -2 to -1‰ and +10 to +22‰ respectively and have only two samples that fall into the Precambrian Limestone field (20AM01A and 20AM08H, Figure 5.11). The remaining samples do not fall into fields defined by previous studies (Bell and Simonetti, 2010).

Marbles group 2 (n = 10) have higher $\delta^{13}C_{PDB}$ and $\delta^{18}O_{VSMOW}$ values, ranging from -1 to +4‰ and +18 to +26‰ respectively. All samples from Marbles group 2 fall into Precambrian and Phanerozoic Limestone fields defined by previous studies (Bell and Simonetti, 2010) (Figure 5.11).

The metadolostone group (n = 1) has the highest $\delta^{18}O_{VSMOW}$ value of all the investigated samples (+26‰) and a $\delta^{13}C_{PDB}$ value of 0‰. It falls into the Precambrian Limestone field on Figure 5.11.

Calcite form nepheline syenite (n = 3) have small ranges of $\delta^{13}C_{PDB}$ and $\delta^{18}O_{VSMOW}$ values that vary from -1 to +1‰ and +12 to +13‰, respectively, and are not associated with any previously defined compositional groups in Figure 5.11.

Calcite-rich rocks group 1 (n = 9) have $\delta^{13}C_{PDB}$ and $\delta^{18}O_{VSMOW}$ values that range from -1 to +2‰ and +11 to +23‰ respectively. Some samples from calcite-rich rocks group 1 (19AM04B1, 19AM04C, 20AM04A, and 20AM12D) fall into Precambrian and Phanerozoic Limestone fields in Figure 5.11.

Calcite-rich rocks group 2 (n = 5) have $\delta^{13}C_{PDB}$ and $\delta^{18}O_{VSMOW}$ values that range from -2 to +2‰ and +12 to +20‰, respectively. Two samples from calcite-rich rocks group 1 (20AM05C and 20AM15B) fall into the Precambrian Limestone field in Figure 5.11.

Samples from calcite-rich rocks group 3 (n = 6) have $\delta^{13}C_{PDB}$ and $\delta^{18}O_{VSMOW}$ values that range from -3 to -1‰ and +10 to +15‰, respectively. Samples from calcite-rich rocks group 3 do not fall into any compositional groups in Figure 5.11.

Amphibole-bearing calcite-rich rocks group 1 (n = 7) have relatively low $\delta^{13}C_{PDB}$ values and a small range of $\delta^{18}O_{VSMOW}$ values, -4 to -2‰ and +12 to +18‰, respectively. One sample in this group (20AM17B) falls into the North American Carbonatite field defined by Bell and Simonetti (2010) (Figure 5.11).

Samples from amphibole-bearing calcite-rich rocks group 2 (n = 5) have slightly higher values ranging from -3 to -1‰. The $\delta^{18}O_{VSMOW}$ values range from +12 to +13‰ for this group, and all samples except one (20AM16A) can be found within the North American Carbonatite field defined by Bell and Simonetti (2010) (Figure 5.11).

Oxygen ratios are compared to Sr concentrations in Figure 5.12. Marbles group 1 and 2 both have similar values to marbles and marble mélange from Moecher et al. (1997). The metadolostone sample is found in the marble field and the nepheline syenite samples are found within the carbonatite field (Figure 5.12). Calcite-rich rocks (amphibole-absent and amphibole-bearing) are widespread and found within several fields defined by Moecher et al. (1997) including carbonatite, marble mélange, and marble.

Table 5.5. Carbon and Oxygen Isotope Ratios

	$\delta^{18}O_{VSMOW}$ (‰)	$\delta^{13}C_{VPDB}$ (‰)
Marble Group 1		
19AM02C	17.76	-2.14
19AM02D1	17.59	-2.25
19AM02D2	17.82	-2.12
20AM01A	18.60	-1.32
20AM01C	12.11	-1.77
20AM06D	10.29	-2.10
20AM08H	22.27	-1.16
Marble Group 2		
19AM01A	23.62	1.73
19AM04A	25.57	2.03
20AM02D	18.15	-1.22
20AM04B	19.62	2.00
20AM05A	19.55	-0.33
20AM05B	24.95	2.40
20AM08I	24.27	0.56
20AM10C	22.77	1.38
20AM13A	25.26	3.54
20AM14B	18.31	2.70
Metadolostone		
20AM11A	25.65	0.03
Nepheline syenite		
19AM05A	12.33	0.59
19AM05B	12.09	-1.30
19AM05C	13.41	0.68
Calcite-rich rocks Group 1		
19AM04B1	21.96	-1.07
19AM04C	21.72	-1.26
20AM03F	16.51	-1.03
20AM04A	15.71	2.46
20AM09A	15.07	1.14
20AM09B	11.40	1.01
20AM09C	12.62	1.86
20AM12D	23.11	-0.62
20AM14A	14.35	1.48
Calcite-rich rocks Group 2		
20AM01D	14.97	-0.06
20AM03E	12.37	-2.10
20AM05C	18.37	-1.46
20AM10B	16.66	-2.15
20AM15B	19.95	1.63
Calcite-rich rocks Group 3		
20AM01B	15.04	-2.48
20AM02A	13.25	-1.44
20AM06A	9.97	-1.37
20AM06B	9.58	-2.58
20AM06C	10.29	-1.75
20AM10A	14.77	-2.03
Amphibole-bearing Calcite-rich rocks Group 1		
19AM02E	14.08	-3.66
19AM02F	15.08	-3.08
19AM03A	16.81	-4.28
20AM08B	17.21	-2.54
20AM08F	18.48	-2.01
20AM16F	11.90	-2.31
20AM17B	14.11	-2.07
Amphibole-bearing Calcite-rich rocks Group 2		
20AM03A	13.08	-2.57
20AM03B	12.87	-2.87
20AM03C	12.93	-2.70
20AM03H	13.08	-2.14
20AM16A	11.88	-1.03

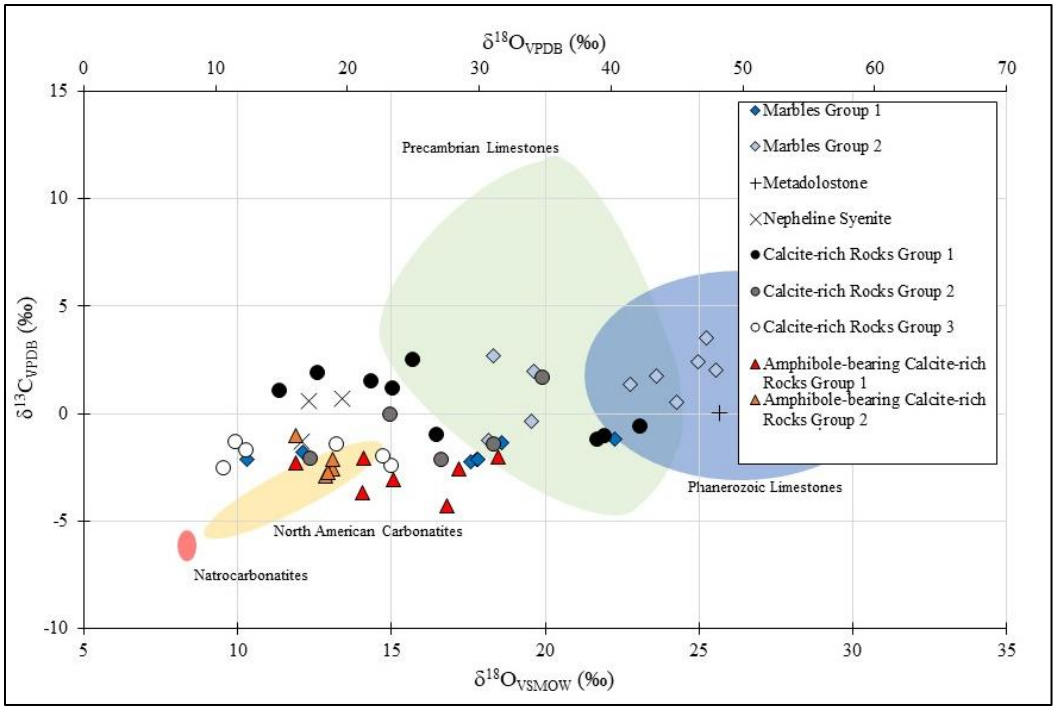

Figure 5.11. Carbon and oxygen isotopic ratios. Shaded regions represent data from Bell and Simonetti (2010).

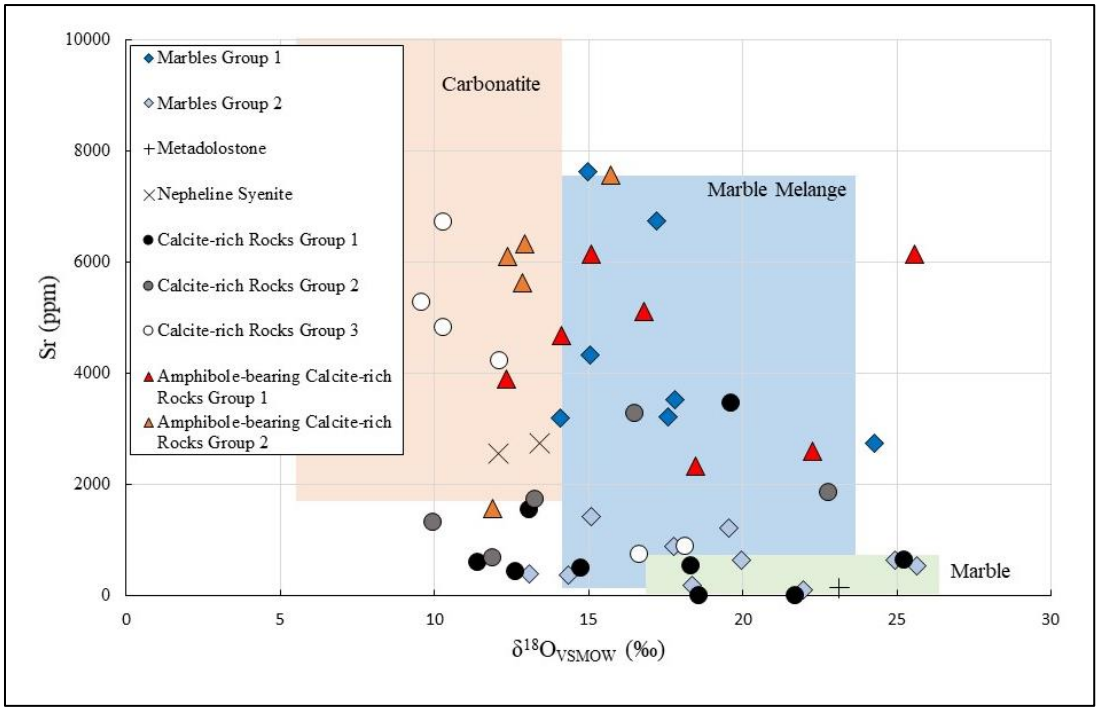

Figure 5.12. Strontium concentrations (ppm) and $\delta^{18}O_{VSMOW}$ (‰). Shaded regions represent data from Moecher et al. (1997).

5.6 Strontium isotope analysis

Eleven samples were selected for strontium isotope analysis (Table 5.6). Marbles group 1 (n = 3) have low $^{87}Sr/^{86}Sr$ values ranging from 0.704106–0.704134 while marbles group 2 (n = 2) have higher $^{87}Sr/^{86}Sr$ values ranging from 0.704815–0.705237. Samples from calcite-rich rocks (n = 3) have higher $^{87}Sr/^{86}Sr$ values ranging from 0.704602–0.705330 than samples from amphibole-bearing calcite-rich rocks (n = 3) that have $^{87}Sr/^{86}Sr$ values ranging from 0.704045–0.704410. The range for carbonatite Sr isotope ratios from the literature is large (0.702-0.705; Gittins et al., 1970) and most of the calcite-rich rocks (amphibole absent and amphibole-bearing) from this study are found within this range, except for sample 19AM04B2 which has the highest $^{87}Sr/^{86}Sr$ value at 0.705353. All calcite-rich rocks have values higher than the average carbonatite (0.7035; Powell, 1966) and the average Ontario carbonatite (0.7028; Powell, 1965). The values from the literature are compared to the findings of this study in Figure 5.13. There is currently no Sr isotope data from the calcite from the metadolostone or nepheline syenite groups.

Table 5.6 Strontium Isotope Ratios

	$^{87}Sr/^{86}Sr$
Marbles Group 1	
19AM02C	0.704134
19AM02D1	0.704112
19AM02D2	0.704106
Marbles Group 2	
19AM01A	0.704815
19AM04A	0.705237
Calcite-rich rocks	
19AM04B1	0.704602
19AM04B2	0.705353
19AM04C	0.704787
Amphibole-bearing Calcite-rich rocks	
19AM02E	0.704133
19AM02F	0.704045
19AM03A	0.704410

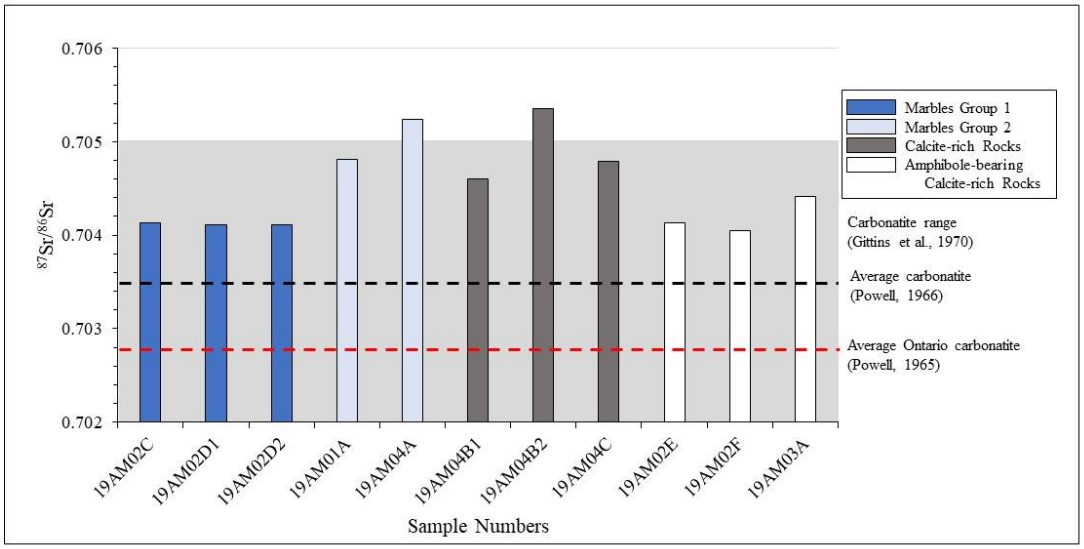

Figure 5.13. Strontium isotopic ratios ($^{87}Sr/^{86}Sr$) for calcite from marble and calcite-rich rocks. Samples are compared to overall carbonatite range (shaded region) (Gittins et al., 1970), the average carbonatite value (black dashed line; Powell, 1966), and the average Ontario carbonatite (red dashed line; Powell, 1965).

6.0 Discussion

6.1 Crystallization of calcite-rich rocks

The genesis of the calcite-rich rocks that appear similar to carbonatites in the Bancroft region (and throughout the wider Grenville Province in general) is a contentious subject (Chiarenzelli et al., 2019; Lentz et al., 1998; Mitchell, 2005). One of the key indicators of petrogenesis of these rocks is whether the preserved mineral assemblage can result from crystallization (equilibrium or fractional) of a carbon-rich liquid (e.g., Slezak and Spandler, 2020; Wyllie and Haas, 1965) or from entrainment of minerals (e.g., Vuorinen and Skelton, 2004). Entrained minerals can be mixed into a magma from the source (e.g., Stevens et al., 2007) or scavenged from wall rock during ascent and after emplacement, i.e., assimilation (e.g., Mitchell, 2009). Entrained minerals will retain their composition from the host rock and can only appear equal to or smaller in size than the minerals in the host rock. This is because they may be partially dissolved after entrainment.

Calcite-rich rocks in Bancroft contain a mineral assemblage of calcite with varying amounts of amphibole, biotite, clinopyroxene, and feldspar (Section 5.2). However, one of the key differences is the grain size. Calcite-rich rocks contain coarse-grained minerals (usually >>5mm) whereas the host rock they are associated with have minerals with smaller grain sizes (normally 1-10mm), so it is unlikely that these minerals are entrained from their host rocks.

The alternative explanation is that the mineral assemblage of the calcite-rich rocks represent crystallization from a carbonate melt. In a silica undersaturated system, which is expected for the calcite-rich rocks at Bancroft due to the absence of quartz, the sequence of nucleation and growth from carbonate liquids in general is expected to be calcite, apatite, oxides, and then silicates (Haynes et al., 2003).

The calcite observed in the calcite-rich rocks is the most abundant mineral and forms large equigranular euhedral crystals (Figure 5.6d). Inclusions of calcite can be found in biotite, pyroxene, and amphibole (if present) (Figure 5.4f). The later minerals tend to be subhedral with varying grain sizes. These factors strongly imply that calcite crystallized earlier than the other minerals and aligns with the crystallization sequence proposed by Haynes et al. (2003) and is generally consistent with the hypothesis that the calcite-rich rocks were produced during crystallization of a mostly carbonate liquid.

6.2 Potential source rocks

Considering that the calcite-rich rocks were more likely derived from the crystallization of carbonate-rich liquid (section 6.1), the source rocks for these liquids can be evaluated using the trace element and isotope data. There are two potential sources for the calcite-rich rocks in the Bancroft region. The first are igneous rocks associated with alkaline and silica-undersaturated magmatism in the region such as nepheline syenite (e.g., Burke et al., 2008; Chayes, 1942; Mungall, 1989) that formed around the timing of Grenvillian orogenesis at 1.1–1.0 Ga (Hanes et al., 1988). The second potential source rocks are metasedimentary rocks (e.g., marbles) that have an affinity with Laurentia and were deposited before Grenvillian orogenesis (probably >1200 Ma; Carr et al., 2000). Below, each of these sources (igneous vs chemical sedimentary origins) is tested using isotopic and trace element data from the calcite-rich rocks in the Bancroft region.

The best comparison for calcite derived from igneous sources in the Bancroft region is primary (i.e., magmatic) calcite hosted by nepheline syenite. Calcite from nepheline syenite rocks in the Bancroft region have high REE values with similar LREE and HREE concentrations (Figure 5.7b) leading to a small La_n/Lu_n value, ranging from 4.2–6.1. This is lower than the values for calcite-rich rocks group 1, group 2, and amphibole-bearing calcite-rich rocks group 1 (Figure 5.8a, b, and Figure 5.9a) which range from 6.1–49.5. La_n/Lu_n values for amphibole-bearing calcite-rich rocks group 2 are similar to the nepheline syenite values (0.8–6.4), but they have much lower concentrations of Sm, Eu, Gd, Tb, Dy, Ho, Er, and Tm (Figure 5.9b). Trace element concentrations are also different between calcite from nepheline syenite and calcite-rich rocks. Amphibole-bearing calcite-rich rocks have generally higher Sr and Ba concentrations than nepheline syenites (n = 9/12 and 6/12 respectively) while amphibole-absent calcite-rich rocks have generally lower Sr and Ba concentrations than nepheline syenites (n = 12/14 and 10/14 respectively) (Figure 5.10).

Therefore, it is unlikely that the calcite-rich rocks were derived from silica undersaturated melts like the nepheline syenites were.

Fractional crystallization of carbonate liquids may lead to residual liquid with variable enrichments of incompatible elements, including U and Th (Le Bas, 1987). Calcite-rich rocks from the Bancroft area are not overly enriched in these elements. For example, calcite from nepheline syenite have concentrations of U that vary from 0.11–3.9 ppm whereas calcite-rich rocks have mostly values <0.2 ppm (n = 27/32). Therefore, it is unlikely that the calcite-rich rocks were fractionated liquids derived from fractional crystallization of a carbonate magma now represented by calcite in nepheline syenite.

In summary, the trace element and REE values of the majority of calcite-rich rocks are unlikely to be derived from an igneous source. This leaves chemical metasedimentary rocks (e.g., metamorphosed limestones or marbles) as a plausible alternative for the source of the carbonate liquids responsible for the calcite-rich rocks in the Bancroft region.

A potential chemical metasedimentary source for the calcite-rich rocks are marbles, which are common in the Bancroft region (Figure 5.1). Two groups of marbles have been identified with different trace element compositions, REE values, and isotope ratios (section 5.3–5.6). Marbles group 1 has relatively high REE values with La_n/Lu_n ratios of 7.6–80.0 and relatively high Sr and Ba concentrations (2730–7630 ppm and 24.7–186 ppm respectively). Marbles group 2 have lower values of La_n/Lu_n ratios of 0.7–20.2 and lower Sr and Ba concentrations (108–1420 ppm and 0.21–37.7 ppm respectively). The isotopic ratios ($\delta^{13}C_{PDB,}$ $\delta^{18}O_{VSMOW,}$ and $^{87}Sr/^{86}Sr$) for Marbles Group 1 are all lower than the isotopic ratios for marbles group 2 (Table 6.1). Similarly, the two separate groups of calcite-rich rocks (amphibole-absent and amphibole-bearing) are defined by differing trace element compositions, REE, and isotope ratios (section 5.3-5.6). Amphibole-bearing calcite-

rich rocks have higher REE, Sr, and Ba concentrations and lower isotopic ratios ($\delta^{13}C_{PDB,}$ $\delta^{18}O_{VSMOW,}$ and $^{87}Sr/^{86}Sr$) than amphibole-absent calcite-rich rocks (excluding calcite-rich Rocks Group 3) and are comparable to the values of marbles group 1 while the amphibole-absent calcite-rich rocks have values that resemble marbles group 2 (Table 6.1). This indicates that the marbles are compatible source rocks for the calcite-rich rocks, but different groups of marbles (with differing geochemical properties) can lead to differing calcite-rich rocks (with different elemental and isotopic compositions). Table 6.1 and Figure 6.1 compares the various isotopic and elemental concentrations for marbles and calcite-rich rocks. In general, the values for the calcite-rich rocks are compatible with those of the marbles.

Considering that igneous rocks are an unlikely source for calcite-rich rocks and the elemental and isotopic similarities between the calcite-rich rocks and the marbles, the mostly likely source for the majority of calcite-rich rocks in the Bancroft region are marbles. Therefore, the majority of calcite-rich rocks in the Bancroft region can be classified as *pseudocarbonatites* (cf. Mitchell, 2005).

One caveat is that a direct comparison of ^{18}O and ^{13}C between potential source rocks (e.g., marbles) and calcite-rich rocks is that it does not consider isotope fractionation. Although fractionation factors for carbon and oxygen between carbonate and carbonate melts are poorly understood (e.g., Knudsen and Buchardt, 1991), the relatively high temperatures (>600 C; Streepey et al., 1997) proposed for metamorphism in the Bancroft area may indicate that isotope fractionation between calcite-carbonate melt were minimal, but this assumption will need to be revisited if new fractionation factors are calculated for calcite-carbonate liquid systems.

Calcite-rich rocks group 3 are samples that do not follow the same REE trends as the rest of the calcite-rich rock samples and are generally anomalous. Four samples in this group

(20AM06A, 20AM06B, 20AM06C, and 20AM01B) have the closest REE patterns to carbonatites from Mungall (1989) and Moecher et al. (1997). These samples fall in and around the carbonatite field for carbon and oxygen isotope ratios (Figure 5.11) and strontium concentrations and oxygen isotope ratios (Figure 5.12). It is possible that these select samples are *carbonatites* (*sensu stricto*) and formed from a silica-undersaturated magma. The other two samples in this group (20AM02A and 20AM10A) have a flat and negative REE slope respectively. The isotope ratios and trace element concentrations for these two samples are more closely related to the other calcite-rich rock samples. It is unclear why the REE patterns are distinct from the other calcite-rich rocks or what the origin of these two calcite-rich rocks are.

Table 6.1. Comparison of elemental and isotope data for different rock types

	Marbles Group 1	Marbles Group 2	Meta-dolostone	Nepheline Syenite	Calcite-rich Rocks*	Amphibole-bearing Calcite-rich Rocks
La_n/Lu_n	8-80	1-20	36	4-6	4-50	1-33
$\delta^{13}C_{PDB}$ (‰)	-2-1	-4-+4	0	-1-+1	-2-+2	-4--1
$\delta^{18}O_{VSMOW}$ (‰)	+10-+22	+18-+26	+26	+12-+13	+11-+23	+12-+18
$^{87}Sr/^{86}Sr$	~0.704	~0.705	N/A	N/A	~0.705	~0.705
Sr (ppm)	2730-7630	110-1420	55	2370-2740	420-3500	1450-6720
Ba (ppm)	25-186	0.21-38	32	58-95	2-149	21-332
K (ppm)	21-360	27-1270	85.5	51-849	11-67	26-81

*Does not include values from calcite-rich rocks group 3

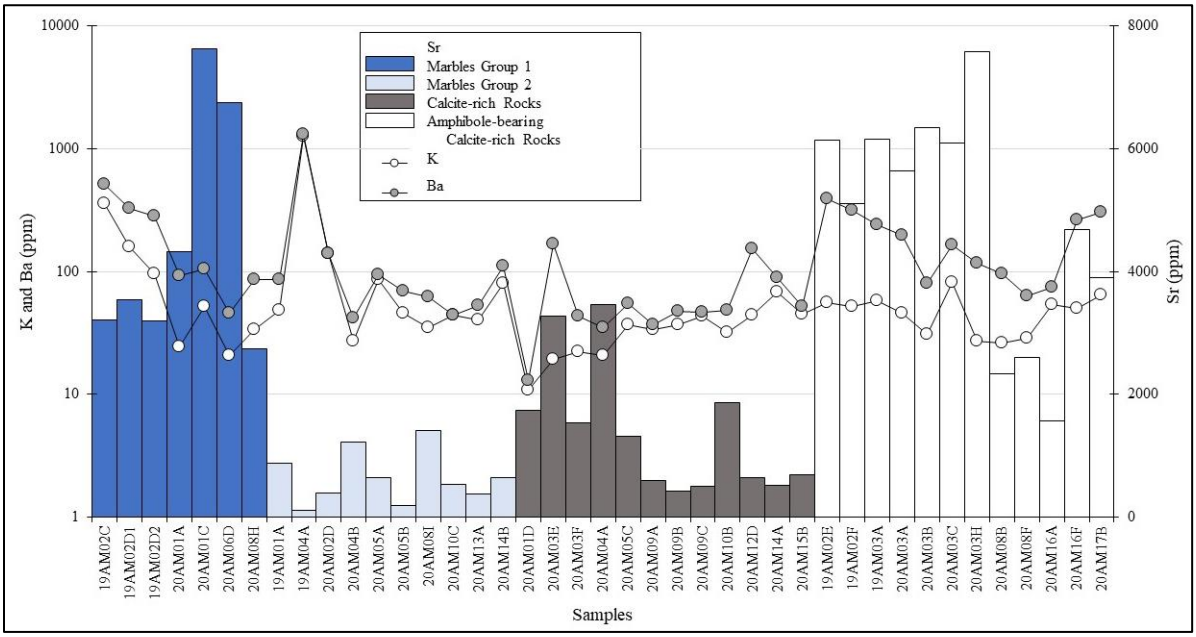

Figure 6.1. Comparison of Sr, K, and Ba concentrations for marbles and calcite-rich rocks.

6.3 Petrogenesis of calcite-rich rocks

The Bancroft calcite-rich rocks studied in this thesis are found in similar areas as the samples from Moecher et al. (1997). Moecher et al. (1997) suggested that these rocks were metamorphosed carbonatites derived from a depleted mantle source. Calcite-rich rocks in our study do not have similar REE patterns and/or concentrations (Figures 5.8 and 5.9) or Sr concentrations and $\delta^{18}O_{VSMOW}$ values (Figure 5.11) when compared to the Moecher et al (1997) samples. The Sr isotopic values of the calcite-rich rocks in this study are too radiogenic to be derived from a depleted mantle source (Figure 6.2). Since the isotopic values and trace element concentrations are incompatible with the carbonatite values from the area and are unlike the mantle sourced calcite from nepheline syenite (section 6.2), it is unlikely that the calcite-rich rocks studied here are true carbonatites. Although a mantle source component cannot be ruled out for the some of the samples investigated here (especially some of the group 3 samples), the differences between calcite in nepheline syenite and from calcite-rich rocks provide further evidence. To recall, calcite from nepheline syenite has smaller La_n/Lu_n values (ranging from 4.2–6.1) and higher concentrations of Sm, Eu, Gd, Tb, Dy, Ho, Er, and Tm (Figure 5.7, 5.8, and 5.9). The isotopic ratios for calcite-rich rocks are widespread but show minimal overlap with values from calcite from nepheline syenite. Amphibole-bearing calcite rocks have generally more depleted $\delta^{13}C_{PDB}$ values than calcite from nepheline syenite (n = 11/12) and amphibole-absent calcite-rich rocks have $\delta^{18}O_{VSMOW}$ values generally more enriched than calcite from nepheline syenite (n = 11/14). Therefore, a mantle source for the calcite-rich rocks investigated in this thesis is unlikely.

The calcite-rich rocks in Bancroft share notable similarities to the silicocarbonate pegmatites in the Adirondacks (Chiarenzelli et al., 2019). The silicocarbonate pegmatite exposures in the Adirondacks show an intrusive origin with veins containing euhedral crystals in a calcite

matrix or pocket that cross-cuts the foliation and compositional layers within host lithologies (Chiarenzelli et al., 2019). This is consistent to the vein-like structures containing calcite-rich rocks in the Bancroft region, southwestern Grenville Province. Carbon and oxygen isotopes were collected from calcite for the Adirondack samples and yielded $\delta^{18}O$ values between +10 and +24‰ and $\delta^{13}C$ values between -3.4 and +0.3‰ (Chiarenzelli et al., 2019). These values are similar to the isotopic ratios from the Bancroft calcite-rich rocks (+11 to +23‰ for $\delta^{18}O_{VSMOW}$ and -4 to +2‰ for $\delta^{13}C_{PDB}$), especially the $\delta^{18}O_{VSMOW}$ values. These samples from the Adirondack silicocarbonate pegmatites and the Grenville Province calcite-rich rocks show isotopic values that range from typical mantle-derived carbonatites to typical carbonate sedimentary rocks. Similar isotopic values in the Grenville are interpreted to be both silicocarbonatites and marble metasomatized by fluids possibly derived from mantle sources (Chiarenzelli et al., 2019; Lentz, 1998; Moecher et al., 1997; Sinaei-Esfahani, 2013). The REE values from Chiarenzelli et al. (2019) are taken from zircon so they are not directly comparable to the calcite REE values from the calcite-rich rocks in Bancroft especially considering that zircon preferentially incorporates HREE over LREE (e.g., Rubatto, 2017).

The main difference between the Adirondacks and Bancroft calcite-rich rocks is the mineral assemblage (Chiarenzelli et al., 2019). The former having voluminous amounts of apatite, silica-undersaturated silicates, betafite, pyrochlore, and uraninite which may be found in the Central Metasedimentary Belt but are not generally coarse grained or abundant (Chiarenzelli et al., 2019). This contrasts with calcite-rich rocks in Bancroft which has an absence of betafite and pyrochlore and has smaller amounts of apatite.

The current hypothesis for the petrogenesis of the Adirondack silicocarbonates is that they were formed by localized anatexis of calc-silicate and marble-rich lithologies of the Grenville

Supergroup (Chiarenzelli et al., 2019). Based on the above similarities in results for the Adirondack silicocarbonates and the Bancroft calcite-rich rocks, their petrogeneses are likely similar. However, the key difference is that there are more marbles in the Bancroft area, and these would generate less silicic liquid than the calc-silicate rocks inferred by Chiarenzelli et al. (2019). This explains the higher abundance of silica-rich minerals in the Adirondack region rocks verses the more calcite-rich varieties in the Bancroft region.

The study area for this thesis lies in the Bancroft Terrane of the Composite Arc Belt in the Grenville Province. There is a possibility that large parts of Bancroft terrane may be from distal Laurentian margin, like metasedimentary rocks (e.g., marbles) (Carr et al., 2000). In this area, carbonate and clastic sediments were deposited between 1300–1250 with an intrusion of tonalitic plutonic rocks (Carr et al., 2000). The tonalitic plutonic rocks are in contact with adjacent marble that were tectonically juxtaposed (>1200 Ma) (Carr et al., 2000). For the metasedimentary rocks to undergo partial melting and produce the calcite-rich rocks, orogenic heating and fluid infiltration is required. This was probably accomplished by orogenic collapse, which creates extensional faults that help facilitate movement and emplacement, as seen in the silicocarbonates of the Adirondacks (Chiarenzelli et al., 2019). Fluxing agents like boron, chlorine, carbon dioxide, and water are made available by the metasedimentary rocks aid in the partial melting of these carbonates (Chiarenzelli et al., 2019). Extensional orogenic collapse was proposed by Rivers and Schwerdtner (2015) for rocks in the Grenville Province in Ontario; these authors also speculated that orogenic collapse allowed the infiltration of fluids into deep levels in the crust.

The Elzevirian Orogeny (1350-1185 Ma) was a compressional orogeny that resulted in overthickened crust and lithosphere which subsequently delaminated causing orogenic collapse (McLelland et al., 1996). The Ottawan orogeny (1080-1040) was a period of convergence causing

the thickening of the pre-Grenvillian Laurentian margin and the Composite Arc Belt (White et al., 2000). This event is interpreted as the main Grenvillian collision causing high-grade metamorphism and deformation throughout the Composite Arc Belt (Jamieson et al., 2010). The widespread ductile deformation and crustal stacking from this orogeny characterizes the Bancroft Terrane (White et al., 2000). Both orogenic events resulted in the transfer of carbonate rocks to depth via thrusting and burial, which was followed by widespread anatexis, allowing metasedimentary rocks to partially melt and produce calcite-rich rocks or pseudocarbonatites. The cross-cutting nature of the calcite-rich rocks leads us to believe they were emplaced late into the tectonic evolution of the area, since there is little to no deformation of these vein-like structures (Figure 5.3a). This is evidential to the hypothesis that the Ottawan orogeny (1080–1040 Ma) was the driving force to produce the calcite-rich rocks in this region. Although the specific timing of carbonate melting and crystallization is unknown, the calcite-rich dykes generally cross-cut fabrics in the rocks that were inferred to have developed during Grenvillian orogenesis. Future work should focus on geochronology of the calcite-rich rocks to determine their absolute ages, and this is described further in section 7.0.

In summary, the petrogenesis of the calcite-rich rocks in the Bancroft area included four potential stages. First the metasedimentary source rocks were deposited and then they were buried and heating during Grenvillian orogenesis. Later, fluid-influx and partial melting of marbles associated with extensional collapse of the Grenville Orogen occurred and lastly, the calcite-rich rocks were mobilized, intruded, and crystallized.

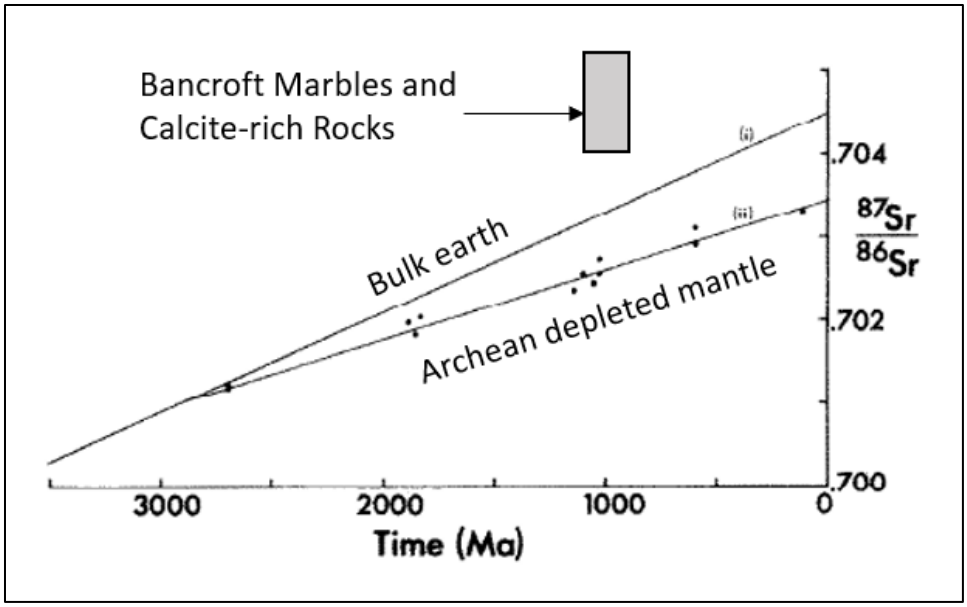

Figure 6.2. Sr isotopic values for bulk earth and Archean depleted mantle modified from Bell and Blenkinsop (1987). The grey shaded region represents results from this study for marbles and calcite-rich rocks from Bancroft, ON.

6.4 Carbon Cycling

The calcite-rich rocks in this study are interpreted to represent melting of carbonate rocks (section 6.3). Although carbonate melting is generally rare, recent studies are starting to find it in more and more places around the world (Ferrero et al., 2016). In the Bancroft region, the fluids necessary for inducing melting of carbonate rocks were probably associated with crustal collapse and fluid flow after Grenvillian orogenesis at *c.* 1.0 Ga. Although the ultimate source of the fluid is not clear, the Grenville orogen is considered a large-hot orogen (Beaumont et al., 2010) and such orogens develop a thermal regime that can allow persistent movement of heat and mass. Such large-scale orogenic systems may be prerequisite for large-scale fluid movement into and out of orogenic systems (e.g., Kerrick and Caldeira, 1998).

There are several large-scale orogenic systems that include the burial and metamorphism of carbonate material. The best Paleoproterozoic example is the Trans-Hudson orogen that extends from the central part of the North American continent to its northeastern edge and orogenesis occurred from 1830-1795 Ma (St-Onge et al., 2006). Although pseudocarbonatites are not known from the Trans Hudson, the similar conditions of metamorphism to the Grenville orogen and the similar magnitude and size suggests that they may be present.

A modern example of a large hot orogen is the Himalayan-Tibetan system (Hodges, 1998). Carbonatite-like rocks (dykes) have been found in the Himalaya and were proposed to be related to melting of carbonate rocks (Liu et al., 2006). In the Himalayan example, interaction of carbonate melt with silicate rocks caused the formation of silicate-rich rocks and the release of CO_2 (Liu et al., 2006). Although the spatial extent of this reaction is unknown, it suggests that melting of carbonate rocks can mobilized carbon both directly (as carbonate melts) and indirectly during melt-rock interaction and CO_2 release. Considering that these reactions take place in the middle crust

and that there is only limited exposure of this crustal level in the Himalaya (e.g., the High Himalaya at the orogenic front), this suggests that carbonate melting, and CO_2 release during melt-rock interaction may be occurring under the modern Tibetan plateau; this represents a potentially very large carbon source for the modern atmosphere. It is generally established that the hot springs in the Tibetan Plateau release CO_2 that was sourced from deep in the crust (e.g., Becker et al., 2008). CO_2 released from the Tibetan Plateau during regional degassing can contribute up to 10% of the global carbon budget (e.g., Newell et al., 2008). Although the mechanisms that generate this CO_2 is not clear, a large proportion is thought to have a deep crustal carbonate origin (e.g., Zhang et al., 2021). This thesis supports the limited previous work that partial melting of metacarbonate rocks has the potential to mobilize CO_2 in the deep crust and the petrogenetic system investigated in the Bancroft domain may have analogues in the deep crust beneath Tibet; this process may represent an overlooked and relatively poorly understood aspect of both ancient (Proterozoic) and modern CO_2 budgets in Earth's atmosphere.

7.0 Future Work

An unknown aspect of the petrogenesis of the calcite-rich rocks in the Bancroft region is their absolute timing of crystallization. Geochronology would be able to determine the age of carbonate liquid crystallization that can better link the petrogenesis of the calcite-rich rocks to the broader evolution of the Grenville orogen. Ages could be obtained using U-Pb zircon or apatite geochronology. Zircon crystals are typically found included in silicate phases (i.e., pyroxenes, amphiboles, micas, feldspar) within these rocks in the Adirondacks (Chiarenzelli et al., 2019) and similar assemblages may be present in the Bancroft region. Zircon is also found in the nepheline syenite phases and if both ages were determined, the presence or absent of timing relationships could be key to understanding if these rocks were crustal or mantle derived. Although apatite is present in the calcite-rich rocks, U-Pb ages obtained from them may not provide the age of crystallization, but of cooling though the closure temperature of Pb in apatite (e.g., Kirkland et al., 2018). Nevertheless, this could still provide a minimum age of calcite-rich rock crystallization and link this age to the various stages of Grenville evolution; in particular if carbonate mobilization occurred during crustal thickening or collapse phase of orogenesis.

8.0 Conclusions

Calcite-rich rocks found in the Bancroft region of the southwestern Grenville Province are pseudocarbonatites due to their elemental and isotopic similarities with the marbles in the region, based off trace element compositions, REE concentrations and patterns, and isotopic ratios; these similarities suggest that the calcite-rich rocks were derived from partial melting of marbles at high temperature. Amphibole-bearing calcite-rich rocks have Sr and Ba concentrations and isotopic ratios ($\delta^{13}C_{PDB}$, $\delta^{18}O_{VSMOW}$, and $^{87}Sr/^{86}Sr$) comparable to samples from marbles group 1, which have higher REE concentrations than other marbles from the area. Amphibole-absent calcite-rich rocks have Sr and Ba concentrations and isotopic ratios ($\delta^{13}C_{PDB}$, $\delta^{18}O_{VSMOW}$, and $^{87}Sr/^{86}Sr$) comparable to samples from marbles group 2, which have comparable REE concentrations to local marbles. Pseudocarbonatites were generated during widespread high-temperature metamorphism that allowed the marbles to partially melt. This was followed by melt mobilization and emplacement that generated the dyke-hosted pseudocarbonatites. The fluids necessary for inducing melting of carbonate rocks were probably associated with crustal collapse and fluid flow after Grenvillian orogenesis at *c.* 1.0 Ga. Carbon movement upwards through the crust may be driven by metamorphism that accompanies large-hot orogens, such as in the Proterozoic Grenville Orogen and in the Cenozoic Himalayan Orogen. This may have important implications for understanding long-term cycling of carbon through Earth's crust. This thesis supports the limited previous work that partial melting of crustal carbonate rocks has the potential to mobilize CO_2 in the deep crust.

References

Agustsson, K. S., Johnston, S. M., Peck, W. H., & Kylander-Clark, A. (2013). Geochemistry and geochronology of the 1.3 Ga metatonalites from the Central Metasedimentary Belt boundary thrust zone in southern Ontario, Grenville Province, Canada. *Geosphere*, *9*(4), 853-863.

Ashwal, L. D., & Wooden, J. L. (1983). Sr and Nd isotope geochronology, geologic history, and origin of the Adirondack anorthosite. *Geochimica et Cosmochimica Acta*, *47*(11), 1875-1885.

Bailey, D. K. (1974). Continental rifting and alkaline magmatism. *The alkaline rocks*, *148*(159), 103-106.

Beaumont, C., Jamieson, R. and Nguyen, M., (2010). Models of large, hot orogens containing a collage of reworked and accreted terranes. *Canadian Journal of Earth Sciences*, *47*(4), pp.485-515.

Becker, J.A., Bickle, M.J., Galy, A. and Holland, T.J., (2008). Himalayan metamorphic CO2 fluxes: Quantitative constraints from hydrothermal springs. *Earth and Planetary Science Letters*, *265*(3-4), pp.616-629.

Bell, K., & Blenkinsop, J. (1987). Archean depleted mantle: evidence from Nd and Sr initial isotopic ratios of carbonatites. *Geochimica et Cosmochimica Acta*, *51*(2), 291-298.

Bell, K., & Simonetti, A. (2010). Source of parental melts to carbonatites–critical isotopic constraints. *Mineralogy and Petrology*, *98*(1-4), 77-89.

Bowen, N.L. (1940). Progressive metamorphism of siliceous limestone and dolomite. *The Journal of Geology*, *48*(3), 225–274.

Bucher, K., & Grapes, R. (2011). *Petrogenesis of metamorphic rocks.* Springer Science & Business Media.

Burke, K., Khan, S.D. and Mart, R.W. (2008). Grenville Province and Monteregian carbonatite and nepheline syenite distribution related to rifting, collision, and plume passage. *Geology*, *36*(12), pp.983-986.

Breemen, O. V., & Currie, K. L. (2004). Geology and U Pb geochronology of the Kipawa Syenite Complex a thrust related alkaline pluton and adjacent rocks in the Grenville Province of western Quebec. *Canadian Journal of Earth Sciences*, *41*(4), 431-455.

Brovkin, V., Sitch, S., Von Bloh, W., Claussen, M., Bauer, E., & Cramer, W. (2004). Role of land cover changes for atmospheric CO2 increase and climate change during the last 150 years. *Global Change Biology*, *10*(8), 1253-1266.

Carlson, K. A., van der Pluijm, B. A., & Hanmer, S. (1990). Marble mylonites of the Bancroft shear zone: Evidence for extension in the Canadian Grenville. *Geological Society of America Bulletin*, *102*(2), 174-181.

Carr, S. D., Easton, R. M., Jamieson, R. A., & Culshaw, N. G. (2000). Geologic transect across the Grenville orogen of Ontario and New York. *Canadian Journal of Earth Sciences, 37*(2-3), 193-216.

Chayes, F. (1942). Alkaline and carbonate intrusives near Bancroft, Ontario. *Bulletin of the Geological Society of America, 53*(3), 449-512.

Chiarenzelli, J., Lupulescu, M., Robinson, G., Bailey, D. & Singer, J. (2019). Age and origin of silicocarbonate pegmatites of the Adirondack Region. *Minerals, 9*(9), p.508.

Craig, H. (1957). Isotopic standards for carbon and oxygen and correction factors for mass-spectrometric analysis of carbon dioxide. *Geochimica et cosmochimica acta, 12*(1-2), 133-149.

Craig, H. (1961). Standard for reporting concentrations of deuterium and oxygen-18 in natural waters. *Science, 133*(3467), 1833-1834.

Davidson, A., Lucas, S. B., & St-Onge, M. R. (1998). An overview of Grenville Province geology, Canadian shield. *Geology of the Precambrian Superior and Grenville provinces and Precambrian fossils in North America. Edited by SB Lucas and MR St-Onge. Geological Survey of Canada, Geology of Canada, 7*, 205-270.

De Bresser, J.H.P., Evans, B. & Renner, J. (2002). On estimating the strength of calcite-rich rocks under natural conditions. *Geological Society, London, Special Publications, 200*(1), pp.309-329.

Durand, C., Baumgartner, L. P., & Marquer, D. (2015). Low melting temperature for calcite at 1000 bars on the join CaCO3-H2O–some geological implications. *Terra Nova, 27*(5), 364-369.

Eamus, D., & Jarvis, P. G. (1989). The direct effects of increase in the global atmospheric CO2 concentration on natural and commercial temperate trees and forests. *Advances in ecological research*, 19, 1-55.

Ellsworth, H. V. (1932). *Rare-element minerals of Canada* (No. 11-12). FA Acland, printer to the king.

Epstein, S.E., Buchsbaum, R., Lowenstaum, H.A., & Urey, H.C. (1953). Revised carbonate-water isotopic temperature scale. *Geological Society of America Bulletin, 64*(11), 1315-1326.

Evans, K. (2011). Metamorphic carbon fluxes: how much and how fast? *Geology*, *39*(1), 95-96.

Ferrero, S., Wunder, B., Ziemann, M. A., Wälle, M., & O'Brien, P. J. (2016). Carbonatitic and granitic melts produced under conditions of primary immiscibility during anatexis in the lower crust. *Earth and Planetary Science Letters*, *454*, 121-131.

Floess, D., Baumgartner, L. P., & Vonlanthen, P. (2015). An observational and thermodynamic investigation of carbonate partial melting. *Earth and Planetary Science Letters, 409*, 147-156.

Gaillardet, J., & Galy, A. (2008). Himalaya--Carbon Sink or Source? *Science, 320*(5884), 1727-1728.

Gittins, J., Hayatsu, A., & York, D. (1970). A strontium isotope study of metamorphosed limestones. *Lithos, 3*(1), 51-58.

Goldschmidt, V.M. (1912). Die Gesetze der Gesteinsmetamorphose mit Beispielen aus der Geologie des Südlichen Norwegens (The laws of rock metamorphism with examples from the geology of southern Norway). *Vi denskapsselskapets Skrifter. 1*.

Hanes, J. A., Clark, S. J., & Archibald, D. A. (1988). An 40Ar/39Ar geochronological study of the Elzevir batholith and its bearing on the tectonothermal history of the southwestern Grenville Province, Canada. *Canadian Journal of Earth Sciences, 25*(11), 1834-1845.

Harker, R.I., & Tuttle, O.F. (1956). Experimental data on the PCO2-T curve for the reaction; calcite-quartz ↔ wollastonite + carbon dioxide. *American Journal of Science, 254*(4), 239–256.

Haynes, E. A., Moecher, D. P., & Spicuzza, M. J. (2003). Oxygen isotope composition of carbonates, silicates, and oxides in selected carbonatites: constraints on crystallization temperatures of carbonatite magmas. *Chemical Geology, 193*(1-2), 43-57.

Hazen, R.M. & Schiffries, C.M. (2013). Why deep carbon? *Reviews in Mineralogy and Geochemistry, 75*(1), 1-6.

Heaman, L. M., Lumbers, S. B., & Vertoli, V. (1988). The timing of carbonatite emplacement within the CMB, Ontario. In *Grenville Workshop 1988, Program and Abstracts*, 11.

Hodges, K.V. (1998). The thermodynamics of Himalayan orogenesis. *Geological Society, London, Special Publications, 138*(1), pp.7-22.

Hoffman, P. F. (1988). United plates of America, the birth of a craton: Early Proterozoic assembly and growth of Laurentia. *Annual Review of Earth and Planetary Sciences, 16*(1), 543-603.

Hoffman, P. F., Bally, A. W., & Palmer, A. R. (1989). Precambrian geology and tectonic history of North America. *The geology of North America Vol. A, The geology of North America—an overview, the geological society of America*, 447-512.

IsoPrime100 User's Guide v1.02 for Ionvantage (2014). IsoPrime Limited, Cheadle Hulme, Cheadle, UK., 219.

IsoPrime MultiFlow User's Guide v1.1 (2014). IsoPrime Limited, Cheadle Hulme, Cheadle, UK., 82.

Jamieson, R. A., Beaumont, C., Warren, C. J., & Nguyen, M. H. (2010). The Grenville Orogen explained? Applications and limitations of integrating numerical models with geological and geophysical data. *Canadian Journal of Earth Sciences, 47*(4), 517-539.

Jones, A. P., Genge, M., & Carmody, L. (2013). Carbonate melts and carbonatites. *Reviews in Mineralogy and Geochemistry, 75(*1), 289-322.

Jutras, P., Macrae, A., Owen, J. V., Dostal, J., Préda, M., & Prichonnet, G. (2006). Carbonate melting and peperite formation at the intrusive contact between large mafic dykes and clastic sediments of the upper Palaeozoic Saint-Jules Formation, New-Carlisle, Quebec. *Geological Journal, 41*(1), 23-48.

Karlstrom, K. E., Harlan, S. S., Williams, M. L., McLelland, J., Geissman, J. W., & Ahall, K. I. (1999). Refining Rodinia: Geologic evidence for the Australia–western US connection in the Proterozoic. *GSA Today*, *9*(10), 1-7.

Keller, J., & Krafft, M. (1990). Effusive natrocarbonatite activity of Oldoinyo Lengai, June 1988. *Bulletin of Volcanology, 52*(8), 629-645.

Kerrick, D.M. and Caldeira, K. (1998). Metamorphic CO2 degassing from orogenic belts. *Chemical Geology, 145*(3-4), pp.213-232.

Kirkland, C.L., Yakymchuk, C., Szilas, K., Evans, N., Hollis, J., McDonald, B. and Gardiner, N.J. (2018). Apatite: a U-Pb thermochronometer or geochronometer? *Lithos, 318*, pp.143-157.

Knudsen, C. and Buchardt, B. (1991). Carbon and oxygen isotope composition of carbonates from the Qaqarssuk Carbonatite Complex, southern West Greenland. *Chemical Geology: Isotope Geoscience section, 86*(4), pp.263-274.

Le Bas, M. J. (1987). Nephelinites and carbonatites. *Geological Society, London, Special Publications, 30*(1), 53-83.

Le Maitre, R. W., Streckeisen, A., Zanettin, B., Le Bas, M. J., Bonin, B., & Bateman, P. (Eds.). (2005). *Igneous rocks: a classification and glossary of terms: recommendations of the International Union of Geological Sciences Subcommission on the Systematics of Igneous Rocks*. Cambridge University Press.

Lentz, D. (1998). Late-tectonic U-Th-Mo-REE skarn and carbonatitic vein-dyke systems in the southwestern Grenville Province. A pegmatite-related pnematolytic model linked to marble melting. *Mineralized intrusion-related skarn systems.*

Lentz, D. R. (1999). Carbonatite genesis: a reexamination of the role of intrusion-related pneumatolytic skarn processes in limestone melting. *Geology*, *27*(4), 335-338.

Li, Y., Zhang, J., Mostofa, K. M., Wang, Y., Yu, S., Cai, Z., ... & Mao, X. (2018). Petrogenesis of carbonatites in the Luliangshan region, North Qaidam, northern Tibet, China: Evidence for recycling of sedimentary carbonate and mantle metasomatism within a subduction zone. *Lithos, 322*, 148-165.

Liu, Y., Berner, Z., Massonne, H.J. and Zhong, D. (2006). Carbonatite-like dykes from the eastern Himalayan syntaxis: geochemical, isotopic, and petrogenetic evidence for melting of metasedimentary carbonate rocks within the orogenic crust. *Journal of Asian Earth Sciences, 26*(1), pp.105-120.

Manabe, S., & Stouffer, R. J. (1980). Sensitivity of a global climate model to an increase of CO2 concentration in the atmosphere. *Journal of Geophysical Research: Oceans*, 85(C10), 5529-5554.

McDonough, W. F., & Sun, S. S. (1995). The composition of the Earth. *Chemical Geology*, *120*(3-4), 223-253.

McLelland, J., Daly, J. S., & McLelland, J. M. (1996). The Grenville orogenic cycle (ca. 1350-1000 Ma): an Adirondack perspective. *Tectonophysics*, *265*(1-2), 1-28.

Miller, R. R. (1984). Tectonic significance of nepheline-bearing rocks in the Haliburton–Bancroft area of the Grenville Province: *Geological Association of Canada*, *9*, 89.

Mitchell, R. H. (2005). Carbonatites and Carbonatites and Carbonatites. *The Canadian Mineralogist*, *43*(6), 2049–2068.

Mitchell, R.H., 2009. Peralkaline nephelinite–natrocarbonatite immiscibility and carbonatite assimilation at Oldoinyo Lengai, Tanzania. *Contributions to Mineralogy and Petrology*, *158*(5), pp.589-598.

Moecher, D. P., Anderson, E. D., Cook, C. A., & Mezger, K. (1997). The petrogenesis of metamorphosed carbonatites in the Grenville Province, Ontario. *Canadian Journal of Earth Sciences*, *34*(9), 1185–1201.

Moyd, L. (1990). Davis Hill near Bancroft, Ontario: An occurrence of large nepheline, biotite, albite-antiperthite crystals in calcite-cored vein-dikes. *Mineralogical Record*, *21*(3), 235–248.

Mungall, J. E. (1989). Geochemistry of Carbonatite and Alkali Pyroxenite, Bancroft Terrane, Grenville Province, Ontario (Master thesis, McGill University Libraries).

Nelson, D. R., Chivas, A. R., Chappell, B. W., & McCulloch, M. T. (1988). Geochemical and isotopic systematics in carbonatites and implications for the evolution of ocean-island sources. *Geochimica et Cosmochimica Acta*, *52*(1), 1-17.

Newell, D.L., Jessup, M.J., Cottle, J.M., Hilton, D.R., Sharp, Z.D. and Fischer, T.P. (2008). Aqueous and isotope geochemistry of mineral springs along the southern margin of the Tibetan plateau: implications for fluid sources and regional degassing of CO2. *Geochemistry, Geophysics, Geosystems*, *9*(8).

Powell, J. L. (1965). Low abundance of Sr87 in Ontario carbonatites. American Mineralogist: Journal of Earth and Planetary Materials, 50(7-8), 1075-1079.

Powell, J. L. (1966). Isotopic composition of strontium in carbonatites and kimberlites. In *Iriternational Mineralogical Association Fourth General Meeting Papers and proceedings, PRJ, Naidu & MN, Viswanathiah (eds)* (pp. 58-66).

Rivers, T., Culshaw, N., Hynes, A., Indares, A., Jamieson, R., & Martignole, J. (2012). The Grenville Orogen–a post-lithoprobe perspective. *tectonic styles in Canada: The lithoprobe perspective*, *49*, 97-236.

Rivers, T. & Schwerdtner, W. (2015). Post-peak evolution of the Muskoka domain, western Grenville Province: ductile detachment zone in a crustalscale metamorphic core complex. *Geoscience Canada: Journal of the Geological Association of Canada/Geoscience Canada: journal de l'Association Géologique du Canada, 42*(4), pp.403-436.

Rubatto, D. (2017). Zircon: the metamorphic mineral. *Reviews in mineralogy and geochemistry, 83*(1), pp.261-295.

Sanford, B. V. & Baer, A.J. (Geological compilation). (1981). MAP 1335A Southern Ontario, Ontario-Quebec-USA [Geologic map]. Retrieved from Geological Survey of Canada, Department of Energy, Mines and Resources.

Sangster, A. L., Gauthier, M., & Gower, C. F. (1992). Metallogeny of structural zones, Grenville province, northeastern North America. *Precambrian Research, 58*(1-4), 401-426.

Sinaei-Esfahani, F. (2013). *Localized metasomatism of Grenvillian marble leading to its melting, Autoroute 5 near Old Chelsea, Quebec* (Doctoral dissertation, McGill University Libraries).

Slezak, P. and Spandler, C. (2020). Petrogenesis of the Gifford Creek Carbonatite Complex, Western Australia. *Contributions to Mineralogy and Petrology, 175*(3), pp.1-23.

Stevens, G., Villaros, A. and Moyen, J.F. (2007). Selective peritectic garnet entrainment as the origin of geochemical diversity in S-type granites. *Geology, 35*(1), pp.9-12.

Stewart, E. M., Ague, J. J., Ferry, J. M., Schiffries, C. M., Tao, R. B., Isson, T. T., & Planavsky, N. J. (2019). Carbonation and decarbonation reactions: Implications for planetary habitability. *American Mineralogist: Journal of Earth and Planetary Materials, 104*(10), 1369-1380.

St-Onge, M.R., Searle, M.P. and Wodicka, N. (2006). Trans-Hudson Orogen of North America and Himalaya-Karakoram-Tibetan Orogen of Asia: Structural and thermal characteristics of the lower and upper plates. *Tectonics, 25*(4).

Streepey, M. M., Essene, E. J., & van der Pluijm, B. A. (1997). A compilation of thermobarometric data from the Metasedimentary Belt of the Grenville Province, Ontario and New York State. *The Canadian Mineralogist, 35*(5), 1237-1247.

Tollo, R. P., Corriveau, L., McLelland, J., & Bartholomew, M. J. (2004). Proterozoic Tectonic Evolution of the Grenville Orogen in North America: Boulder, Colorado, Geological Society of America Memoir 197.

Vuorinen, J.H. and Skelton, A.D. (2004). Origin of silicate minerals in carbonatites from Alnö Island, Sweden: magmatic crystallization or wall rock assimilation?. *Terra Nova, 16*(4), pp.210-215.

Wenzel, T., Baumgartner, L. P., Brügmann, G. E., Konnikov, E. G., Kislov, E. V., & Orsoev, D. A. (2001). Contamination of mafic magma by partial melting of dolomitic xenoliths. *Terra Nova, 13*(3), 197-202.

White, D. J., Forsyth, D. A., Asudeh, I., Carr, S. D., Wu, H., Easton, R. M., & Mereu, R. F. (2000). A seismic-based cross-section of the Grenville Orogen in southern Ontario and western Quebec. *Canadian Journal of Earth Sciences, 37*(2-3), 183-192.

Whitney, D. L., & Evans, B. W. (2010). Abbreviations for names of rock-forming minerals. *American mineralogist, 95*(1), 185-187.

Woolley, A. R., & Kjarsgaard, B. A. (2008). Paragenetic types of carbonatite as indicated by the diversity and relative abundances of associated silicate rocks: evidence from a global database. *The Canadian Mineralogist, 46*(4), 741-752.

Wyllie, P. J., & Haas Jr, J. L. (1965). The system CaO-SiO2-CO2-H2O: 1. Melting relationships with excess vapor at 1 kilobar pressure. *Geochimica et Cosmochimica Acta, 29*(8), 871-892.

Yakymchuk, C., Rehm, A., Liao, Z. and Cottle, J.M., (2019). Petrochronology of oxidized granulites from southern Peru. *Journal of Metamorphic Geology, 37*(6), 839-862.

Zhang, M., Guo, Z., Xu, S., Barry, P.H., Sano, Y., Zhang, L., Halldórsson, S.A., Chen, A.T., Cheng, Z., Liu, C.Q. and Li, S.L. (2021). Linking deeply-sourced volatile emissions to plateau growth dynamics in southeastern Tibetan Plateau. *Nature Communications, 12*(1), pp.1-10.

Appendices

Appendix A – Trace element concentrations of reference materials

Water Reference Materials

T207

		Replicates						
	accepted	1	2	3	4	5	average	%RD
K (ppm)	2.19	2.00	2.09	2.11	2.16	2.17	2.11	-3.8
V	0.938	0.84	0.88	0.86	0.87	0.87	0.86	-7.9
Co	0.976	0.93	0.95	0.91	0.91	0.90	0.92	-5.8
Ni	1.74	1.64	1.68	1.64	1.63	1.67	1.65	-5.0
Sr	161	149.07	153.42	154.51	159.36	159.79	155.23	-3.6
Mo	4.62	4.34	4.31	4.29	4.18	4.17	4.26	-7.8
Ba	42.9	39.51	39.67	39.43	39.79	39.32	39.54	-7.8
Pb	4.8	4.76	4.79	4.73	4.79	4.72	4.76	-0.8
U	1.8	1.69	1.70	1.70	1.72	1.68	1.70	-5.6

T211

		Replicates						
	accepted	1	2	3	4	5	average	%RD
K (ppm)	0.979	0.89	0.92	0.92	0.95	0.97	0.93	-5.0
V	1.87	1.76	1.78	1.73	1.78	1.77	1.76	-5.6
Co	2.07	2.01	2.01	1.97	1.98	2.01	2.00	-3.5
Ni	2.23	2.29	2.31	2.27	2.31	2.30	2.30	3.0
Sr	134	125.92	126.72	127.48	132.17	134.84	129.43	-3.4
Mo	1.1	0.99	1.01	0.97	1.01	0.99	0.99	-9.9
Ba	55	49.76	50.47	49.83	50.89	50.22	50.23	-8.7
Pb	1.66	1.61	1.61	1.58	1.61	1.61	1.60	-3.4
U	0.6	0.56	0.57	0.55	0.57	0.56	0.56	-6.3

Appendix A *continued*

T225

		Replicates						
	accepted	1	2	3	4	5	average	%RD
K (ppm)	2.5	2.23	2.27	2.34	2.39	2.40	2.32	-7.0
V	12.9	11.77	11.68	11.76	11.87	11.80	11.77	-8.7
Co	1.07	0.94	0.95	0.94	0.93	0.94	0.94	-12.3
Ni	6.89	6.87	6.80	6.86	6.88	6.78	6.84	-0.8
Sr	730	669.62	676.85	698.71	715.62	724.68	697.10	-4.5
Mo	1.8	1.66	1.68	1.64	1.62	1.61	1.64	-8.8
Ba	118	107.90	110.02	109.50	108.56	109.02	109.00	-7.6
Pb	4.27	4.26	4.29	4.26	4.24	4.24	4.26	-0.3
U	9.52	9.07	9.07	9.01	8.98	9.06	9.04	-5.1

T231

		Replicates						
	accepted	1	2	3	4	5	average	%RD
K (ppm)	1.36	1.28	1.29	1.33	1.35	1.35	1.32	-3.0
V	2.9	2.71	2.70	2.70	2.67	2.68	2.69	-7.2
Co	1.53	1.45	1.43	1.43	1.43	1.39	1.43	-6.9
Ni	0.7	0.63	0.63	0.63	0.62	0.61	0.62	-10.8
Sr	254	237.59	240.08	246.46	252.26	252.06	245.69	-3.3
Y	0.108	0.10	0.10	0.10	0.10	0.10	0.10	-7.1
Mo	0.74	0.64	0.63	0.64	0.66	0.65	0.64	-13.1
Ba	89.8	81.82	81.76	82.60	83.41	82.82	82.48	-8.1
La	0.286	0.28	0.26	0.27	0.27	0.27	0.27	-5.9
Ce	0.408	0.40	0.40	0.40	0.39	0.39	0.39	-3.5
Pr	0.077	0.07	0.07	0.08	0.07	0.07	0.07	-3.2
Nd	0.305	0.29	0.27	0.28	0.28	0.29	0.28	-7.8
Sm	0.048	0.05	0.05	0.04	0.05	0.05	0.05	-2.1
Gd	0.039	0.04	0.04	0.04	0.04	0.03	0.04	-7.2
Dy	0.021	0.02	0.02	0.02	0.02	0.02	0.02	-19.6
Er	0.01	0.01	0.01	0.01	0.01	0.01	0.01	-10.0
Pb	3.71	3.68	3.65	3.65	3.68	3.60	3.65	-1.5
U	2.37	2.25	2.22	2.22	2.22	2.19	2.22	-6.4

RD: relative difference

Appendix B – Average detection limits for QQQ-ICP-MS

Detection Limits (ppm)

	Detection Limit
P	6.105
K	2.926
Ti	0.3588
V	0.004578
Co	0.003768
Ni	0.01818
Rb	0.01471
Sr	0.005712
Y	0.001632
Zr	0.05504
Mo	0.050206
Ba	0.006118
La	0.0005204
Ce	0.0009939
Pr	0
Nd	0.003647
Sm	0
Eu	0
Gd	0.003535
Tb	0.0003314
Dy	0.00136
Ho	0.0003379
Er	0.001638
Tm	0.0002687
Yb	0
Lu	0.0002938
Hf	0.04912
W	0.0561
Re	0.002542
Pb	0.004871
Th	0.2166
U	0.00139

Appendix C – Chondrite Values

Chondrite Values	
	Detection Limit
La	0.237
Ce	0.613
Pr	0.0928
Nd	0.457
Sm	0.148
Eu	0.0563
Gd	0.199
Tb	0.0361
Dy	0.246
Ho	0.0546
Er	0.16
Tm	0.0247
Yb	0.161
Lu	0.0246

Chondrite values are from McDonough and Sun (1995).